UPPSALA
UNIVERSITET

Heterometallic Oxo-Alkoxides of Europium, Titanium and Potassium

ERIK BERGER

Department of
Materials Chemistry
Licentiate Thesis
2010

Heterometallic oxo-alkoxides of europium, titanium and potassium

Thesis for the degree of licentiate of philosophy in inorganic chemistry presented at Uppsala university in 2010

Coordination compounds of europium and titanium with oxide, ethoxide (OCH_2CH_3), *iso*-propoxide ($OCH(CH_3)_2$) and *tert*-butoxide ($OC(CH_3)_3$) ligands have been studied. These belong to the general class of oxo-alkoxides, $M_xO_y(OR)_z$, with alkoxide ligands (OR) containing an organic, aliphatic part R. The R group can be systematically varied, permitting the investigation of the influence of electronic and steric effects on the coordination of metal and oxygen atoms. Their tendency towards hydrolysis and formation of metal-oxygen-metal bridges also makes (oxo)alkoxides interesting as precursors in liquid solution-based or gas phase-based synthesis of many technologically important materials.

The structure of a termetallic oxo-alkoxide of formula $Eu_3K_3TiO_2(OH/OCH_3)(OR)_{11}(HOR)$ ($R = C(CH_3)_3$) was revealed by a combination of single-crystal X-ray diffraction and IR spectroscopy. Its unusual structure features a facial oxygen-centered Eu_3K_3O octahedron sharing one face with an oxygen-centered K_3TiO tetrahedron. Six-coordination of oxygen by a combination of alkali metal and lanthanoid atoms is not uncommon for alkoxides, but the attachment of a tetrahedron to one of its faces provides a new dimension to the library of oxo-alkoxide structures. The structure was the result of incomplete metathesis in the synthesis attempt of europium-titanium oxo-*tert*-butoxides.

$Eu_4TiO(OR)_{14}$ and $(Eu_{0.5}La_{0.5})_4TiO(OR)_{14}$ ($R = CH(CH_3)_2$) were found to be isostructural with previously published $Ln_4TiO(OR)_{14}$ structures (Ln=Sm, $Tb_{0.9}Er_{0.1}$). X-ray diffraction and UV-Vis absorption results show no site preference for La in either the solid state or hexane solution. The $Ln_4TiO(OR)_{14}$ structure forms part of an interesting group of $Ln_4MO(OR)_{10+z}$-$(HOR)_q$ structures where M is another lanthanoid (Ln) or a di-, tri- or tetravalent heteroatom, giving either a square pyramidal or a trigonal bipyramid-like coordination of the central oxygen atom, depending on the chemistry and size of M.

$Eu_2Ti_4O_2(OR)_{18}(HOR)_2$ ($R = CH_2CH_3$) was deduced from IR data to have the same molecular structure as $Er_2Ti_4O_2(OR)_{18}(HOR)_2$. UV-Vis measurements are also in agreement with the presence of one symmetry-unique europium site in the molecular structure. Structure determination by single-crystal X-ray diffraction has yet to be performed.

Erik Berger, Department of Materials Chemistry, Ångström Laboratory, Uppsala University, Box 538, SE-752 21 Uppsala, Sweden

List of papers

This thesis is based on the following papers, which are referred to in the text by their Roman numerals.

I Structure of a hepta-nuclear termetallic oxo-alkoxide:
$Eu_3K_3TiO_2(OBu^t)_{11}(OMe/OH)(HOBu^t)$
(Erik Berger and Gunnar Westin)
Journal of Sol-Gel Science and Technology **53(3)** (2010) 681-688.

II Structure of $Eu_4TiO(OCH(CH_3)_2)_{14}$ and $Eu_2La_2TiO(OCH(CH_3)_2)_{14}$ and spectroscopic studies of three Eu-Ti alkoxides: $Eu_4TiO(OCH(CH_3)_2)_{14}$, $Eu_2La_2TiO(OCH(CH_3)_2)_{14}$ and $Eu_2Ti_4O_2(OC_2H_5)_{18}(HOC_2H_5)_2$
(Erik Berger and Gunnar Westin)
In manuscript

My contribution to papers **I** and **II** consists of all experimental work except the melt-sealing of capillaries, all measurements and processing of data, and a large part of the experimental planning, the writing and the visualisation of results.

Errata list for paper I

Fig. 2: O14 should read O15 and O15 should read O14.

Nomenclature

The following symbols for alkyl/alkoxide groups are used in this thesis:

R	Any alkyl group, such as CH_3, also including ether-alkyl groups like $CH_2CH_2OCH_3$.
Me	CH_3 = methyl-
Et	CH_2CH_3 = ethyl-
^{n}Pr	$CH_2CH_2CH_3$ = *n*-propyl-[1]
^{i}Pr	$CH(CH_3)_2$ = *iso*-propyl-[1]
^{t}Bu	$C(CH_3)_3$ = *tert*-butyl-

In the results section, the compounds are numbered with numerals in bold type:

1	$Eu_3K_3TiO_2(OH/OMe)(O^tBu)_{11}(HO^tBu)$
2	$Eu_4TiO(O^iPr)_{14}$
3	$(Eu,La)_4TiO(O^iPr)_{14}$
4	$Eu_2Ti_4O_2(OEt)_{18}(HOEt)_2$

Other symbols and abbreviations used:

BVS	Bond valence sum(s)
EDS	Energy dispersive X-ray spectroscopy/spectrometry
IR	Infrared / Absorption spectroscopy in the infrared range
Ln	Lanthanoid element (occasionally including scandium and yttrium)
μ_n	Bridging *n* metal atoms (as in μ_3-O = triply bridging oxo ligand)
moe	$OCH_2CH_2OCH_3$ = methoxy-ethoxo ligand
moeH	$HOCH_2CH_2OCH_3$ = methoxy-ethanol
SCXRD	Single-crystal X-ray diffraction
SEM	Scanning electron microscope/microscopy
t	Terminal (as in t-OR = terminal alkoxo ligand
THF	$O[CH_2]_4$ = tetrahydrofuran
UV-Vis	Ultraviolet-Visible / Absorption spectroscopy in the ultraviolet to visible range

[1] not to be confused with the element praseodymium, Pr:
$Pr_4TiO(O^iPr)_{14}$ = oxo-tetradekakis(*iso*-propoxo)-tetra-praseodymium-titanium

Table of Contents

1. Introduction

Much of modern society is built around, if not dependent on, lots of technological devices relying on the specific properties of materials, which can be electronic, magnetic, optical, etc. For the most part, these functional materials have been designed for their specific purposes, possessing structures or elemental compositions that do not correspond to those found in natural sources. Thus, they need to be synthesised from two or more components.

The most traditional synthesis methods for multicomponent materials are based on the reactions between solid components at elevated temperatures. For the cases where melting temperatures are inappropriate (too high or coinciding with high volatilities), these methods generally suffer from slow kinetics and insufficient mixing at the atomic scale [1,2]. Also, high-temperature solid-state techniques restrict the product materials mainly to those that are thermodynamically stable. Moreover, many technologically important devices are based on precisely shaped materials at the nano scale, such as thin films, sponges and nanoparticles, and such materials cannot be prepared by conventional methods. Therefore, a wealth of other techniques have been developed where the reactants or intermediates are not solids/melts, but atoms, ions or molecules in liquid solution, gas phase or plasma phase, allowing for intimate mixing before condensation to the solid state [2].

1.1 Sol-gel synthesis

One general method for the synthesis of functional materials is the sol-gel method, which is based on the mixing of components in liquid solution before gradual densification to solid materials [2-3]. The name is derived from the aggregation states that are passed during the transformation from the initial solutions of small entities to the solid networks in the final product: a sol is a dispersion of large colloidal particles, and a gel is characterised by the coexistence of an infinite solid network and an infinite liquid network (fig. 1). Sometimes, however, the term sol-gel is also used for related solution-based methods that do not strictly pass through the sol and gel stages.

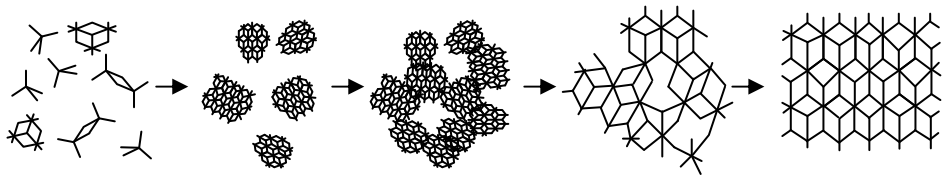

Fig. 1 Schematic drawing of the sol-gel route: solution → sol → gel → amorphous solid → crystalline solid.

The sol-gel method can in particular be used for the synthesis of advanced oxide ceramics, and often affords pure and homogeneous materials where other methods fail. The explanation for this is the atomic-scale mixing of precursors and the often lower temperatures required to obtain the final product. A drawback is that a successful sol-gel method to a specific material may require a lot of engineering as well as knowledge about the structures of the precursors, reaction paths etc., and precursors may be expensive.

1.2 Alkoxides and oxo-alkoxides

Alkoxide ions are the conjugate bases of alcohols, and metal alkoxides are the coordination compounds formed between metal ions and alkoxide ligands (fig. 2, 4a-d). Since alcohols are only weak acids, alkoxide ions are strong bases, and metal alkoxides tend to hydrolyse under condensation and elimination of alcohol when exposed to water (fig. 3).

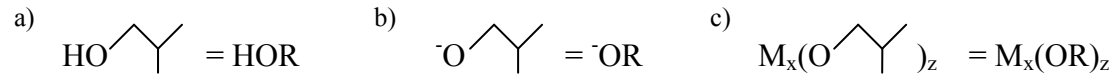

Figure 2 a) Alcohol = hydrocarbon chain with a hydroxyl group b) Alkoxide ion = deprotonated alcohol c) Metal alkoxide = coordination compound with alkoxide ligands.

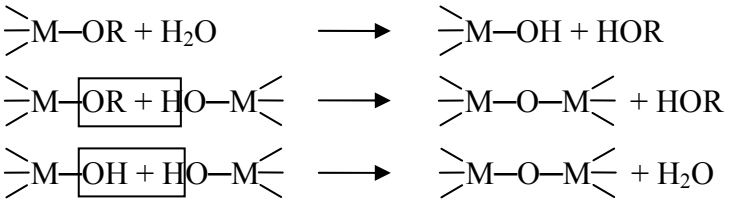

Figure 3 Some possible hydrolysis and condensation reactions for metal coordination centres with alkoxide ligands.

Alkoxides are highly versatile precursors for sol-gel synthesis [2, 4]. In contrast to, e.g., nitrates or carboxylates, alkoxides condensate under formation of volatile alcohols and/or ethers, allowing for the formation of pure products without impurities due to the precursor ligands. Also in metal-organic chemical vapour deposition (MOCVD), alkoxides are sometimes used as precursors [5-6].

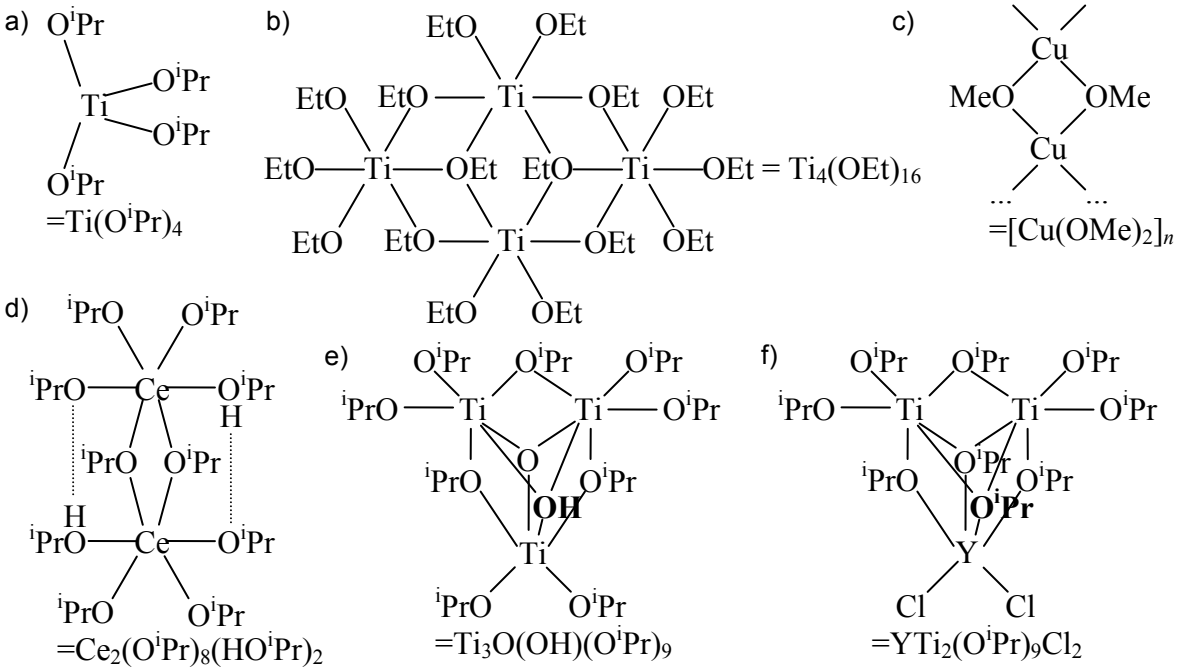

Figure 4 Examples of alkoxide derivatives: a) monomer [7] b) oligomer [8] c) polymer [9] d) alcohol-adducted alkoxide [10-11] e) oxo-hydroxo-alkoxide [12] f) chloro-alkoxide [13].

Many so-called alkoxides are in fact oxo- or hydroxo-alkoxides (fig. 4e), which are the condensation and/or hydrolysis products of true alkoxides. In oxo-alkoxides one or more centrally placed bridging oxo ligands help increase the coordination number of the metal atoms; in some cases, these form spontaneously from true alkoxides, presumably under ether or alkene elimination, whereas in other cases hydrolysis is needed. They can also be the result of oxidation by e.g. O_2. The reactivity of oxo-alkoxides decreases with the ratio of (bridging) oxo to alkoxo ligands, and polyoxoalkoxides can be regarded as small fragments of alkoxide-terminated metal oxide.

Alkoxide derivatives may also contain other ligands, such as chloride ions or organic non-alkoxide ligands. Chloro-alkoxides often adopt structures similar to alkoxide structures (such as that in fig. 4f), but are normally avoided in sol-gel synthesis, since the chloride ions tend to remain in the gel after hydrolysis and appear as impurities in the final materials. By contrast, modification with bidentate organic groups such as acetyl acetonate, rendering the complexes less reactive in one or several directions and favouring gelation over precipitation, is quite common in sol-gel synthesis [4]. However, the lower reactivity of these groups may also imply that oxides prepared from modified alkoxides are in general less pure than those prepared from unmodified alkoxides, hydroxo-alkoxides or oxo-alkoxides. Therefore, other ligands than alkoxide, oxide and hydroxide will not be further considered here.

Within this thesis, the term "alkoxides" may refer either to complexes containing only alkoxide ligands or to oxo- and/or hydroxo-alkoxides.

Apart from being important precursors in materials synthesis, alkoxides are also interesting from a structural point of view. For example, the choice of alkyl group provides a means of systematic variation for the investigation of coordination chemistry around metal and oxygen atoms. Other parameters that can be systematically varied are the nuclearity and number of oxo bridges. This means that the hydrolysis and condensation pathways of alkoxides can in fact be studied step by step, in contrast to, e.g., condensation pathways through thermal decomposition.

1.3 The lanthanoids and lanthanoid alkoxides

The lanthanoids[2] are interesting as dopants in many functional materials. Although consisting of a complete series in the periodic table, namely that in which the 4f shell is filled, they behave very much like one single group because of the low extent to which the 4f electrons participate in chemical bonding. Especially in the predominant oxidation state of +III, corresponding to the release of two s-electrons and one d-electron, there is a great similarity and exchangeability. This is contrasted by a large variation in atomic properties such as ionic radius[3], the lanthanoids being such a large group. This can be exploited both in structural stability studies and in the tailoring of dimension-dependent properties, such as piezoelectricity [14]. The 4f electrons also give rise to magnetic and optical properties which lend themselves to use in applications like displays [15], frequency-converters [16] and biomarkers [17].

[2] The lanthanoids are defined by IUPAC as the fifteen elements with atomic numbers 57 through 71 (La-Lu), but in this thesis, whenever f electrons are not involved, the 3d elements scandium and yttrium may occasionally be referred to by the same term; in particular Y(III) behaves chemically just like any other trivalent lanthanoid.

[3] The systematic decrease in size throughout the 4f series is not remarkable itself, but as it spans over as many as 15 elements, the total effect is a large contraction (the "lanthanoid contraction"), to such an extent that the early 5d elements are similar in size to their 4d congeners.

In addition to the general chemical equivalency of the lanthanoids, some of the 4f elements have variable oxidation states, reflecting the tendency to achieve (nearly) empty, half-filled or filled f shells. In oxidation states +IV (Ce, Pr) and +II (Sm, Eu, Yb), these ions are in fact more similar to group 4 or group 2 species, such as Zr(IV) or Sr(II) respectively.

The alkoxide-based sol-gel method lends itself particularly well to the synthesis of lanthanoid-containing materials, which are often metastable. The often low temperatures needed for conversion of gel to oxide can prevent diffusion and reaction to more thermodynamically stable phase-separated structures. For instance, on Er-doping of silica glasses for signal amplification in optical fibres, the erbium atoms tend to form erbium oxide-rich domains. These processes occur fast already above 200°C and are detrimental to the material's optical properties. The use of heterometallic alkoxides in sol-gel synthesis, keeping the lanthanoid elements separated in the gel by optically inactive atoms such as Si, Ti or Al, has been proven to circumvent this problem [18].

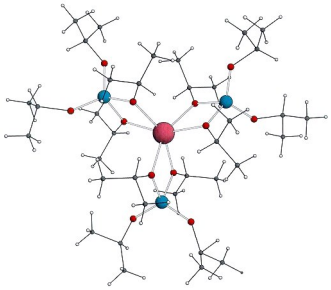

Heterometallic $ErAl_3$ alkoxide used for Er doping of optical fibres [18]

The combination of lanthanoid elements and alkoxides thus leads to an interesting research field, comprising fundamental aspects of coordination chemistry, as well as the possible applicability of the compounds studied. Apart from being possible sol-gel or MOCVD precursors, lanthanoid alkoxides can also act as single-molecular magnets [19] or as catalysts in organic synthesis [20].

For the full exploitation of alkoxides it is essential to gain structural knowledge about alkoxides of varying nuclearity, degree of hydrolysis etc. From existing structural information, conclusions can be drawn about possible new structures, suitable as materials precursors, and about reaction pathways in sol-gel synthesis. For the trivalent lanthanoid alkoxides, precise structural knowledge has been gained only rather recently. With most work stemming from the last two decades, much remains to be explored [21].

1.4 Scope of this thesis

This thesis focuses on heterometallic alkoxides of trivalent lanthanoids and titanium, in particular of europium and titanium. Trivalent europium takes a special place among the lanthanoids because of its spectroscopic properties described in section 2.2. The tendency of europium to form divalent species will not be dealt with in this thesis.

Previously, heterometallic lanthanoid titanium alkoxide structures have been reported with ethoxide (-OEt = $-OCH_2CH_3$) and *iso*-propoxide ($-O^iPr = -OCH(CH_3)_2$) ligands [22-26]. For erbium, the binary "$Ln(OR)_3$"[4]-$Ti(OR)_4$ and ternary "$Ln(OR)_3$"[4]-Ln_2O_3-$Ti(OR)_4$ systems were investigated in more detail [22-23].

In the system "$Ln(OEt)_3$"-$Ti(OEt)_4$ (Ln=Er), IR and UV-Vis spectroscopy showed the presence of erbium and titanium ethoxides which, however, could not be isolated in the form of crystals [22]. When allowing the formation of oxo-alkoxides through hydrolysis (and in very low yields also without hydrolysis on heating), the heterometallic oxoalkoxide

[4] To date, the structures of "$Ln(OEt)_3$" and "$Ln(O^iPr)_3$" are not known.

$Er_2Ti_4O_2(OEt)_{18}(HOEt)_2$ was obtained and could be structurally characterised. For Er:Ti ratios below 1:2, the same product was obtained, along with titanium ethoxide. The structure has not yet been reported for other lanthanoids.

In the system "$Ln(O^iPr)_3$"-$Ti(O^iPr)_4$ (Ln=Er), IR spectroscopy again showed evidence of unstable erbium and erbium titanium non-oxo alkoxides [23]. By contrast, the oxo-alkoxide structure $Ln_4TiO(O^iPr)_{14}$ has been reported for Ln=Sm [24], $Tb_{0.9}Er_{0.1}$ [26], $La_{0.5}Er_{0.5}$ [27], Pr [25] and Er [23] (the first three refined by X-ray crystallography and the latter two indicated by IR spectroscopy). With erbium, Er:Ti ratios below 4:1 were shown to lead to the formation of $Er_4TiO(O^iPr)_{14}$ as well as $Ti(O^iPr)_4$ [23].

The present studies on europium-titanium alkoxides have been performed in three main directions:
1) reproduction of structures previously reported for other lanthanoids
2) investigation of other alkoxide ligands
3) increased degree of hydrolysis

This thesis summarises the results of the four syntheses listed in table 1. The syntheses conducted with *tert*-butoxide ligands led to a new structure, presented in paper I. The syntheses conducted with ethoxide and *iso*-propoxide ligands reproduced the same structures as previously reported for other lanthanoids. The exploration of how the combination of visible range spectroscopy and lanthanoid substitution can contribute to the future assignment of new structures led to the results presented in paper II.

Table 1. Syntheses included in this thesis.

Alkyl group	Target stoichiometry	Hypothesis / Question	Obtained	Paper
Et	$Eu_2Ti_4O_2(OEt)_{18}$	Isostructural with $Er_2Ti_4O_2(OEt)_{18}(HOEt)_2$	Same molecular structure	II
^{i}Pr	$Eu_4TiO(O^iPr)_{14}$	Isostructural with $Ln_4TiO(O^iPr)_{14}$ (Ln=Sm, $Er_{0.1}Tb_{0.9}$)	Same crystal structure: $Eu_4TiO(O^iPr)_{14}$ ($I4_1cd$)	II
^{i}Pr	$Eu_2La_2TiO(O^iPr)_{14}$	Site preference?	Random distribution: $(Eu_{0.5}La_{0.5})_4TiO(O^iPr)_{14}$	II
^{t}Bu	$Eu_2TiO(O^tBu)_8$	Composition and structure of alkoxide(s)?	$Eu_3K_3TiO_2(O^tBu)_{11}$-(OMe/OH)(HO^tBu)	I

The resulting compounds were examined with a combination of IR and UV-Vis spectroscopy and X-ray diffraction and their structures compared with their respective homologues as well as other related compounds.

2. Methodology

2.1 Synthesis

Overview of common alkoxide synthesis methods

Table 2 summarises some common synthesis routes to homometallic alkoxides [5, 21, 28]. Metal dissolution (eq. 2.1 in Table 2) is most suitable for the most electropositive metals. Lanthanoids also react with alcohol, but may need refluxing conditions and/or a catalyst. Moreover, yields are normally significantly less than 100% due to formation of hydrides as well as of multiple oxidation stages for several of the lanthanoids. Alcoholysis (eq. 2.2) of alkyl- and especially silylamides has been very popular, since these are very reactive towards alcohols, and their conjugate acids often have low lewis acidity and high volatility. A drawback is the extensive purification needed before the amides can be used. Alcoholysis attempts with halides generally only lead to partial alcoholysis or to alcohol adducted halides

instead of alkoxides. For some metal chlorides, such as $TiCl_4$, the alcoholysis reactions can be driven to completion with the help of a proton-acceptor like NH_3 (eq. 2.3), whereas lanthanoid chlorides react to completion only with alkali metal alkoxides, in the metathesis reaction described in the next paragraph. Transesterification reactions between alkoxides and esters (eq. 2.6) have also been reported.

Table 2. Some common routes to homometallic alkoxides.

Metal dissolution in alcohol	$M(s) + z\ ROH \rightarrow M(OR)_z + z/2\ H_2(g)\uparrow$	*(2.1)*
Alcoholysis of other complexes (hydrides, alkyls, amides, alkylamides, silylamides, pyridyls, halides, other alkoxides, ...)	$ML_z + z\ ROH \rightarrow M(OR)_z + z\ HL(g)\uparrow$ (L=H, R, NH_2, NR_2, $N(SiR_3)_2$, py, X, OR', ...)	*(2.2)*
Alcoholysis of halide, base-driven	$MX_z + z\ HOR + z\ NH_3 \rightarrow M(OR)_z + z\ NH_4X(s)\downarrow$	*(2.3)*
Metathesis between halide and alkali metal alkoxide	$MX_z + z\ AOR \rightarrow M(OR)_z + z\ AX(s)\downarrow$	*(2.4)*
	$MX_z + z\ LiOR \rightarrow M(OR)_z(s)\downarrow + z\ LiX$	*(2.5)*
Transesterification reactions	$M(OR')_z + z\ MeCOOR \rightarrow M(OR)_z + z\ MeCOOR'$	*(2.6)*

In the halide-alkoxide metathesis reaction, the target alkoxide is most commonly soluble in nonpolar solvents, and Na or K is chosen as the alkali metal, giving insoluble NaX or KX (eq. 2.4). If the target alkoxide is less soluble than lithium halide, lithium alkoxides can be used instead (eq. 2.5). This type of metathesis reaction may be slower than alcoholysis of amides, but this is outweighed by the ease with which pure alkali metal alkoxides are prepared by metal dissolution as a starting step (eq. 2.1). In fact, the lanthanoid amides are produced by an analogous halide-amide metathesis (using alkali metal amide) anyway, so if the halide-alkoxide metathesis works, there is really no need to go through the extra amide steps. One reason might be to avoid the formation of chloro-alkoxides $M(OR)_{z-x}X_x$ or alkali metal-containing mixed-metal alkoxides $MA_x(OR)_{z+x}$, but if the constituents are properly mixed and care has been taken that proper stoichiometries are used, this only happens in a few cases [28]. Therefore, the metathesis route is our method of choice.

Table 3 lists a few routes to heterometallic alkoxides. Whereas several pairs of metal alkoxides react with each other to give the corresponding heterometallic alkoxides (eq. 2.7 in Table 3), many other combinations give either sluggish reactions or unwanted reactions. Again, metathesis reactions where one metal introduced as halide is allowed to displace alkali metal from mixed metal alkoxides (eq. 28), have turned out to provide a simple, well-functioning alternative, which gives good control over stoichiometry.

Table 3. Some common routes to heterometallic alkoxides.

Mixing of alkoxides	$M(OR)_z + x\ M'(OR')_{z'} \rightarrow MM'_x(OR)_z(OR')_{xz'}$	*(2.7)*
Metathesis between halide and alkali metal heterometallic alkoxide	$MX_z + z(x/y)\ AM'_y(OR)_{1+yz'}$ $\rightarrow MM'_x(OR)_{z+xz'} + z(x/y)\ AX(s)\downarrow$	*(2.8)*

Control of oxo ligand content

As mentioned in the introduction, oxo-alkoxides may or may not be the result of deliberate or unintended hydrolysis. In many cases, it has been proven possible to isolate non-hydrolysed alkoxides apart from the reported oxo-alkoxides, but as a result of lower stabilities due to the tendency to associate solvent molecules in absence of oxo ligands, few such non-oxo alkoxides have been completely structurally characterised.

In the pursuit of oxo-alkoxides, the best yields are therefore obtained when stoichiometric amounts of water are added to the reaction solutions in a controlled manner. Not adding water deliberately may also yield oxo-alkoxides, but in less predictable yields, depending on many factors such as the water content of the solvents, the dryness of the glove-box atmosphere, the reaction temperature, the skill of the experimenter or any factor related to chemical

equilibrium for the cases where oxo-formation occurs even in the total absence of water. In the present studies of oxo-alkoxides, water was always added, diluted in organic solvents.

Synthesis procedure

The syntheses were performed under anhydrous conditions, using anhydrous chemicals (except for water) and dry glassware in a glove-box containing dry argon (<1 ppm O_2, H_2O). PTFE-coated stirring magnets were used, as well as PTFE-lined NS ground glass joints, but rubber stoppers with septa were also frequently used.

The identities and structures of products and intermediates were determined using a combination of infrared absorption spectroscopy (section 2.2), UV-Vis absorption spectroscopy (section 2.3) and single-crystal X-ray diffraction (section 2.4).

Elemental analysis was performed using energy-dispersive X-ray spectroscopy (EDS) in a scanning electron microscope (SEM) at various stages of the syntheses. Samples, taken both from liquid phases and from crystals or sediments, were air-hydrolysed and dried prior to analysis. This simple procedure assumes that hydrolysis is sufficiently fast and the volatility of the sample (constituents) sufficiently low to preclude evaporation. The assumption may have been invalid whenever (volatile) unreacted titanium alkoxides were present in reaction mixtures, but in these cases, the exact titanium contents were not important.

All syntheses were performed in the same order, using the alkali metal alkoxide / lanthanoid chloride metathesis route combined with controlled hydrolysis. Mixtures of the respective alcohol and toluene were used as solvents during the syntheses, whereas alcohol/hexane solutions were sometimes used for crystallisation and for characterisation.

	Synthesis step	**Result**
1.	Treatment of potassium with alcohol	Potassium alkoxides
2.	Addition of titanium alkoxide	Alkoxide mixtures or mixed-metal alkoxides
3.	Addition of diluted water	Formation of oxo-alkoxides
4.	Addition of $LnCl_3$	Metathesis: precipitation of KCl
5.	Centrifugation	Sediment-free liquid phase
6.	Evaporation of solvent, sometimes followed by solvent replacement (evaporation + solvent addition)	Crystallisation

After step 5, the liquid phases were analysed for Ln, K, Ti and Cl contents as an indication of the success of the metathesis reactions. In most cases, the liquid phases were free of potassium and chlorine and rich in lanthanoid and titanium, but for attempts with the *tert*-butoxide ligand, this was not the case and the reactions were given longer time, both at room temperature and at 60°C. Even then, potassium was still always present in the liquid phase, and for one composition, a solution containing both Eu, K and Ti was used in the subsequent steps 5 and 6, which eventually led to the isolation and structure determination of $Eu_3K_3TiO_2(OR)_{12}(HOR)$ as described in section 3.2.

Evaporation of solvent was usually initiated by evacuation. The connection to the pump (with cold trap) was effectuated by rubber hoses and either ground glass joints or a needle through the septum of a rubber stopper. Slow evaporation of toluene and hexane was achieved by leaving the flasks for a time with rubber stoppers. Large or small crystals developed within short time for $Eu_3K_3TiO_2(OR)_{12}(HOR)$, $Eu_4TiO(OR)_{14}$ and $Eu_2La_2TiO(OR)_{14}$. Most attempts to crystallise $Eu_2Ti_4O_2(OEt)_{18}(HOEt)_2$ led to platelet-shaped crystals adhering to the walls of the glassware.

Synthesis challenges

Since the compounds under study contain organic groups, there is a plethora of possible side reactions. Apart from hydrolysis, one can imagine oxidation-reduction, dehydrogenation and many other reactions, which can be avoided only with great experimental skill and experience, high purity chemicals and favorable laboratory conditions. Some sources of contamination encountered in this work are:

- the heat generated by the dissolution of potassium in alcohol, accelerating the decomposition of solvent molecules (alcohols, toluene). A compromise has to be found between temperature increase (rapid alcohol addition) and risk for alcohol deficience (slow alcohol addition), possibly leading to decomposition of the potassium alkoxides formed.
- the basicity of potassium alkoxides, increasing the risk for unwanted reactions. Reaction mixtures should not stand for long time between the metal dissolution step and the lanthanoid chloride addition.
- the solvent evacuation steps. Unpredicted boiling (bumping) may bring the reaction media in contact with the rubber stoppers or even with the rubber hoses used for evacuation; perhaps more commonly, the cold trap is blocked by frozen alcohol, heaving the pressure difference between rubber hose and reaction flask. Trouble-free solvent evacuation demands long experimental experience.
- the rubber stoppers, which may react either with reaction mixtures, when in accidental contact, or with solvent vapours. Reflux-like condensation is suspected to have occurred at times, with the concomitant risk of rubber constituents leaking down into the reaction mixtures. Thus, the use of rubber stoppers is to be avoided, especially for long-time storage.

Since the oxo-alkoxides under study were only moderately soluble in their parent alcohols, the alcohols were in general employed to free crystals and powders from alcohol-soluble contaminations.

Other problems include the softness of crystals due to the non-polar organic groups at the outside of each molecule. This often results in difficulties to collect crystalline material without destroying its crystallinity. Also, cutting of crystals may introduce deformations.

Since the alkoxides are susceptible to hydrolysis, single crystals for X-ray diffraction experiments have to be protected in sealed capillaries. The insertion of the soft crystals into the capillaries is tedious work: shoving of the crystals along the capillary walls must be avoided to any extent, since this would imply a risk for deformation, as well as for crystal traces impairing the melt-sealing of the crystals in the form of soot. Instead, the crystals are carefully inserted on the tip of a thin copper wire, and paraffin oil is added to make the crystals stay in place. For alkoxides suspected to contain alcohol adducts, it is also recommended to surround the crystals by a slight amount of alcohol to avoid decomposition.

2.2 Spectroscopy

Infrared (IR) spectroscopy

For lanthanoid alkoxides, FTIR absorption spectroscopy has proven useful as a tool for the identification of structural analogues where one lanthanoid element has been substituted for another [23, 25]. Below 1300 cm^{-1}, a rough assignment of peaks as being due to C-O, C-C and M-O vibration modes can also be made, and this was used to corroborate the structural models refined from the single-crystal X-ray diffraction data.

For the compounds under study, IR spectra were measured between polished KBr discs. Solid samples were smeared out in nujol, a paraffin with few IR absorption peaks of its own. In some cases, liquid samples were dried on KBr, with or without nujol, before measurement. Spectra for these dried samples match those recorded for crystals.

Ultraviolet-Visible (UV-Vis) spectroscopy

For trivalent 4f ions, observed colours are mainly[5] due to the absorption of visible light by electronic f-f transitions [29-31]. The 4f electrons can be compared with the 3d electrons in 3d ions. Both are shielded by the outer-shell s and p electrons and can to a first approximation be regarded as belonging to free ions. In free (monatomic) ions, d-d and f-f transitions are strictly forbidden by Laporte's selection rule and, moreover, many transitions are forbidden by the intercombination rule as well (spin-forbidden). However, the surrounding ligands do affect the 3d and 4f electrons sufficiently to bring about:

1) distortion from even symmetry by uneven (such as tetrahedral, trigonal prismatic) coordination or uneven vibrational modes, making Laporte's rule hold less strictly
2) a weakening of the intercombination rule through electronic coupling
3) changes in energy levels, and therefore in absorption energies
4) a broadening of absorption bands due to ligand vibration.

For the 3d elements, these effects lead to d-d absorption bands of intermediate intensity, substantially broadened as compared to atomic spectral lines, and (in absence of strong non d-d absorption bands) to a large variety in colour, even for one and the same element in a given oxidation state. The 4f electrons of Ln^{3+} ions, on the other hand, interact much less with ligand fields. Thus, each Ln^{3+} has a characteristic f-f absorption spectrum, with narrow bands of low intensity, especially those corresponding to spin-forbidden transitions. Nevertheless, f-f absorption bands are often strong enough to be observed by UV-Vis spectroscopy, and their fine structures and intensities do vary with ligand field, allowing for differentiation between different structures.

Among the trivalent lanthanoids, a special case arises for Eu^{3+} [32]. The ground states of all other lanthanoids for which f-f transitions are possible (thus excluding La^{3+} and Lu^{3+}, which have an empty and a filled f shell, respectively), have non-zero total angular momentum quantum number *J*. In non-symmetrical environments, states with non-zero *J* are split, and therefore also the f-f transitions from the ground state will in principle be split, resulting in several fine peaks for each transition. Eu^{3+}, on the other hand, has a non-degenerate ground state ($^7F_0$), as well as a non-degenerate excited state ($^5D_0$). This means that any observed splitting of the $^5D_0 \leftarrow {}^7F_0$ transition must be caused by different Eu^{3+} sites. Europium is therefore often used as a site probe, especially where trivalent lanthanoids can be exchanged for each other without alteration of the chemical and structural environments: if Eu^{3+} is distributed over a certain number of sites in a structure, other lanthanoids with sufficiently similar radii can be assumed to behave similarly. In conclusion, in the case of molecular compounds such as alkoxides, UV-Vis spectroscopy for Eu^{3+} provides more easily-interpreted information than for the other lanthanoids, for which the technique rather serves as a fingerprint method.

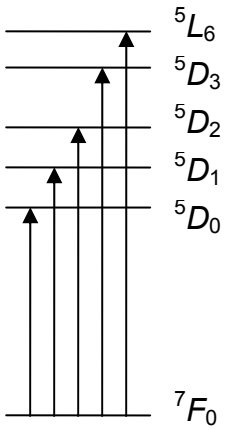

Fig. 5 Some f-f transitions from the Eu^{3+} $^7F_0$ ground state

At room temperature, apart from the ground state, there is a small population of $^7F_1$ and $^7F_2$ excited states, which are close in energy. The transitions from the ground state shown in fig. 5, are therefore accompanied by weak absorption bands at slightly lower energy / longer wavelength due to excitation from $^7F_1$ and $^7F_2$.

[5] For Ce^{3+} and Tb^{3+}, as well as for divalent Ln^{2+} (e.g. Eu^{2+}), f-d transitions also have energies in the visible range. In contrast to f-f transitions, f-d transitions are not forbidden by quantum-chemical selection rules, and cause broad absorption bands and strong colours [Hol]. On illumination of Ln^{3+} by white light, weak f-f luminescence may also result in apparent colours [G1].

UV-Vis absorption spectra were recorded in the range of about 350 to 600 nm for hexane solutions in sealed cuvettes of either fused quartz/silica or infrasil.

2.3 Single-crystal X-ray diffraction (SCXRD)

All single-crystal diffraction experiments were performed on crystals up to 1 mm in diameter, protected inside melt-sealed glass capillaries prepared under argon atmosphere. Intensity data were collected as ω-2θ scans on a diffractometer equipped with an area detector. During data collection, the crystals were cooled by a stream of dry air, which was slowly cooled to 170K before the measurements.

After extraction of preliminary information (diffraction symmetry, unit cell parameters and orientation) based on a small portion of reflexions, all reflexion intensities were integrated and corrected for Lorentz and polarisation effects using the SAINT software (Bruker AXS).

Empirical "absorption" corrections were applied by the program SADABS, based on the intensity spreads for groups of symmetry-equivalent reflexions among the highly redundant data. The program is designed to identify and correct for apparent systematic errors, including but not limited to absorption by the crystal. For the examined crystals, absorption is in fact of minor importance; rather, the large crystal sizes and irregular shapes cause a variation in irradiated sample volume as a function of crystal orientation. Other examples of systematic errors are absorption by the supporting capillary, incident beam inhomogeneity and crystal decay. Judging from diagnostic plots (fig. 6), the fluctuation of diffracted beam intensity as a function of orientation was indeed a major factor.

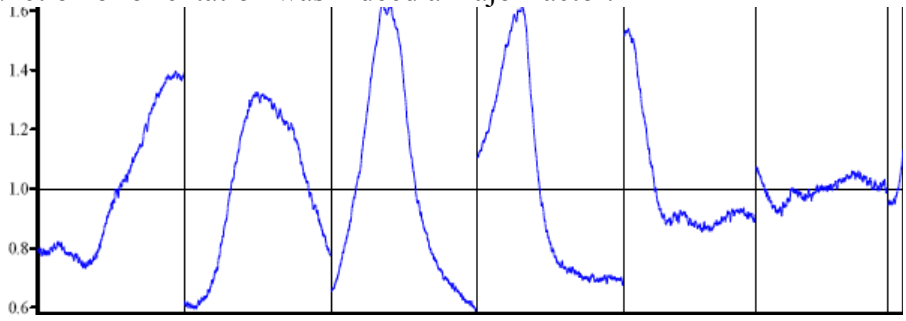

Fig. 6 Variation of overall scale factor from SADABS-correction for $Eu_2La_2TiO(O^iPr)_{14}$ data set, with omega scans at different phi angles. Since the curves are discontinous between scans, the variation is attributed to fluctuations in the crystal volume covered by the X-ray beam (depending on crystal orientation), rather than to fluctuations in incoming beam intensity.

A new program was written for the creation of diagnostic plots, complementary to those provided by SADABS. The integrated reflexion data (by SAINT) contain, for each reflexion, the HKL indices, phi, omega, time etc., as well as six "direction cosines", describing the orientation of the diffracted beam with respect to the diffractometer. Although the definitions of the direction cosines are not given in the documentation, it can be seen that especially the even-numbered cosines make good coordinates for the representation of data in outlier plots. These plots show the reflexions that deviate the most in intensity from their equivalent reflexions, in terms of $(I-\langle I\rangle)/\sigma$, where I and σ are the intensity and estimated standard uncertainty for each reflexion and $\langle I\rangle$ is the $1/\sigma^2$-weighted mean intensity for all equivalent reflexions. For most data sets, these plots confirm the success of the SADABS correction, as shown for the $Eu_2La_2TiO(O^iPr)_{14}$ data set in fig. 7.

In one case (the $Eu_3K_3TiO_2(OR)_{12}(HOR)$ data set used for structure refinement), the new plots revealed a systematic decrease in intensity which SADABS was not able to correct for, since it was confined to a small part of the two-dimensional space defined by two of the

direction cosines. Nevertheless, reflexions in the middle of this area were on average weakened to as low as 30% of the intensities of equivalent reflexions, and it was judged justified to remove this part of this "direction cosine space" (not related to reciprocal space) before correction by SADABS. For better statistics and reliability, the weighted mean intensities <*I*> were this time based on all equivalent reflexions in three data sets normalised to a common scale (the data set used for structure refinement was still given the largest weights as its standard uncertainties were smaller). Medians of $(I-\langle I\rangle)/\sigma$ were calculated over squares of 0.04x0.04 in the second and fourth direction cosines, and after graphical evaluation of the medians (fig. 8), less than 2% of all data were cut out from the data, reducing the number of unique reflexions by less than 0.2%. It was later confirmed in the structure refinement that this indeed improved the quality of the model.

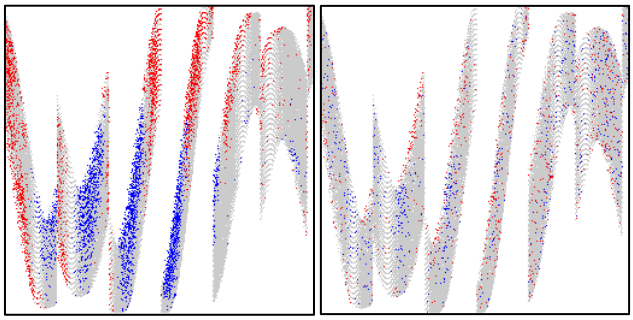

Fig. 7 Outlier plots for $Eu_2La_2TiO(O^iPr)_{14}$ data set, before and after correction by SADABS (without rejection of outliers). Red dots are reflexions with $(I-\langle I\rangle)/\sigma>2$, blue dots reflexions with $(I-\langle I\rangle)/\sigma<-2$. The horizontal axis is time (cf. fig. 6) and the vertical axis is the fourth "direction cosine".

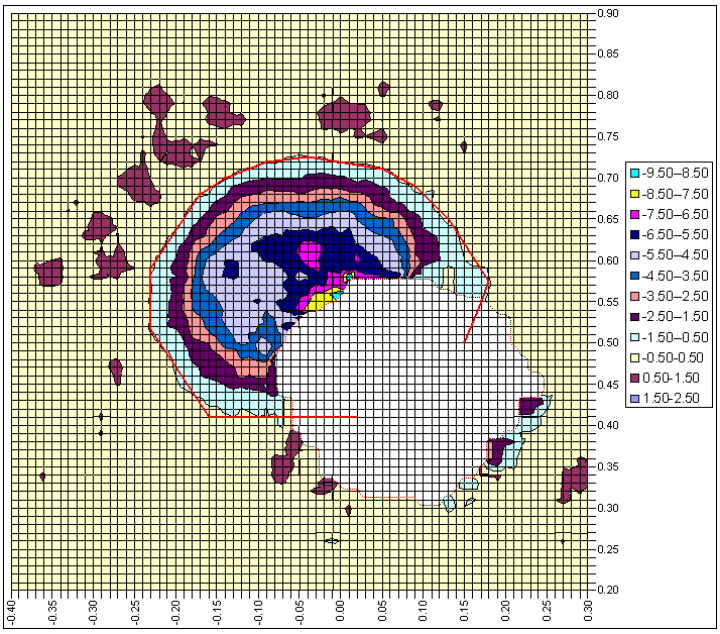

Fig. 8 Contour plot of $(I-\langle I\rangle)/\sigma$ used for the location of bad data in the $Eu_3K_3TiO_2(OR)_{12}(HOR)$ data set (with direction cosines 2 and 4 as coordinates). The red border shows where the data were cut, closely following the contour line for median$((I-\langle I\rangle)/\sigma)=-0.5$. The "hole" in the middle of the picture is a part of space where no reflexions were measured at all. Medians calculated in the immediate vicinity of the hole are therefore based on few reflexions and random errors may increase/decrease the medians locally, as in the bottom right of the picture.

The structures were solved using direct methods, yielding probable positions for the heavy atoms, identified as lanthanoid or other metal atoms. For $Eu_2La_2TiO(O^iPr)_{14}$, the Patterson function was used as an extra check on the non-separability of Eu and La. Refinement was based on F^2 for all data and the structural models were successively extended by adding oxygen and carbon atoms based on difference electron density peaks, and later anisotropic displacement factors for all non-hydrogen atoms. Site disorder was refined when the underlying residual electron density peaks made geometrical and chemical sense. Hydrogen atoms attached to carbon were finally added in idealised positions, such that their positions followed those of the carbon atoms at fixed lengths and angles in the further refinement ("riding model").

2.4 Structure determination and analysis

Determination/identification of non-hydrogen atomic structure

The determination of structures is a priori based on the X-ray diffraction data as described in 2.3. However, for the cases where no diffraction data have been collected, the good agreement found between infrared absorption spectra for alkoxides which differ only in the identity of the lanthanoid, can be taken as a strong indication of identical molecular structures, as described in 2.2.

The combination of infrared and UV-Vis spectroscopy was also used as a second check on the validity of the structural models found by the X-ray diffraction method.

Determination of metal oxidation states and hydrogen atom positions

Hydrogen atoms attached to carbon can sometimes be found from residual electron density, as described (for larger atoms) in section 2.3. But neither the assessment of oxidation states of the metal atoms, nor the location of hydrogen atoms attached to O, can in general be refined from X-ray diffraction data. Instead, one must look at other signs, such as sample coloration, presence of OH bands in infrared spectra, and analysis of bond lengths and angles. Thus, Eu^{2+} causes a strong yellow colour as well as a lengthening of Eu-O bonds compared to Eu^{3+}. Protons attached to oxygen also cause a lengthening of metal-oxygen bonds and should, in addition, cause a distortion around the oxygen atoms. A qualitative way of comparing bond lengths is provided by the BVS method described below.

The BVS method

The bond valence sum (BVS) method [33] is based on the concept of bond valences and their approximation from observed bond lengths. The calculated bond valences and their sums can be used as checks on the validity of structural models. Bond valences also facilitate the comparison between homologous structures with different cations or anions.

The central theorem of the BVS method is the valence sum rule, which states that the sum of bond valences around a cation or anion must always be equal to its valence (equation 2.9). Theoretical bond valences can be shown to be proportional to the electrostatic fluxes between cations an anions regarded as point charges. However, the calculation of these fluxes is not straightforward and bond valences must instead be approximated from experimental data.

$$V_i = \Sigma_j v_{ij} \qquad (2.9)$$

The underlying assumption for the use of bond lengths is that there exists a simple relation between bond valence and bond length. For most bonds between metal cations and chalcogenide/halide anions, two-parameter expressions such as equations 2.10 or 2.11 turn out to be sufficient (often even with the b parameter in equation 2.10 kept constant at a "universal" value), whereas especially H-O bonds are subject to a more complicated relation. Based on large sets of crystallographically determined structures, average bond valence parameters (R_0, b), or less frequently (R_0, N), have been determined and tabulated for many element pairs. Usually, the parameters have been determined for cations and anions in specific oxidation states (e.g., Eu(III)-O(II) vs. Eu(II)-O(II)), but attempts to derive oxidation state-independent parameters have also been made. For some 3d transition metals, a division can also be made between high-spin and low-spin states. There is still debate as to whether such divisions should be made or not, and to whether it is justifiable to regard b as a universal constant. For proper answers to these questions, large amounts of structural data are needed. With the growing volumes of structural databases [34] future improvements of the empirical data sets are still to be expected.

$v_{ij} = \exp[(R_{ij}-R_0)/b]$, R_0 and b constant for the bond type in question (*2.10*)
$v_{ij} = (R_{ij}/R_0)^{-N}$, R_0 and N constant for the bond type in question (*2.11*)

Although developed for typical ionic structures, the bond valence model has proven successful also for molecular coordination complexes, and it is said that the ionic or covalent character of a bond is irrelevant [33]. However, bonds must always be between atoms with positive and negative formal charge, and therefore the method cannot be applied to many organic or metallic compounds [33].

The BVS method can be used to determine oxidation states of both cations and anions as well as protonation states of anions. Before the development of the BVS method, Pauling's second rule, dividing the cation valences equally over the surrounding bonds, giving Pauling bond strengths summing up to approximative anion valences (equation 2.12), helped mineralogists decide on whether for instance an oxygen atom was an O^{2-} ion (V_{anion}~2) or rather an OH^- ion (V_{anion}~1) [33, 35]. However, when coordination numbers decrease, as for ligands of molecular compounds, the approximative nature of Pauling's second rule becomes clear. Also, Pauling's method is less satisfactory when inversed for the calculation of cation valences in order to determine oxidation numbers. The notion that there is a strong correlation between Pauling's bond strengths and bond lengths eventually led to the formulation of the BVS method, which allowed for unequal distribution of the cation's valence over its bonds (fig. 9), and indeed proved much more accurate in the reproduction of valences of both cations and anions. Among other merits of the BVS method can be mentioned the distortion theorem, which can explain distortions from ideal cation or anion environments in terms of changes in BVS values. The classical example is the small "rattling" titanium cation moving off-centre in perovskites, thereby raising its bond valence sum [33].

$V_{anion} = \Sigma p_j$, $p_j = V_j/N_j$, where V_j is the valence (ionic charge) and N_j the coordination number of cation j (*2.12*)

The BVS method explains why bonds to bridging ligands are usually longer than bonds to terminal ligands, and the more metal atoms a ligand bridges, the longer its bonds to the metal atoms, since the same bond valence sum is to be distributed over a growing number of bonds (often expressed as t-O < μ-O < μ_3-O < ...). But it can also explain deviations from this trend: figure 9 shows how two bridging OR ligands can be distributed equally or unequally over two metal atoms. In both cases, the bond valence sums for the metal atoms and the OR ligands are the same (1.0), but in the second case, the bond lengths can vary substantially although all bond lengths are of one type (metal to doubly bridging ligand). Thus, one of them may accidentally be longer than another bond to a triply bridging ligand.

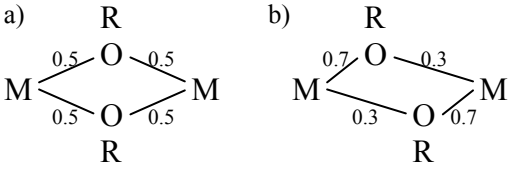

Figure 9. Two hypothetical $M_2(OR)_2$ structural fragments with a) equal b) unequal distribution of bond valences. In a) and b), all Pauling bond strengths would be equal.

Being an empirical method, the BVS method must be used with great care. One must ensure that the bonds are comparable to those for which parameters were derived. If, e.g., Fe(II)-O(II) parameters were calculated from low-spin complexes only, they should not be used for high-spin Fe(II) complexes. Also, since homopolar bonds cannot be described by the BVS method, bond valence parameters for "cationic" carbon are necessarily based on

structures where carbon is surrounded by atoms that can be regarded as anions, and must therefore be used only for similar bonding situations (acetates, carbonyls, etc.). In addition, the published bond valence parameters suffer from several uncertainty factors, as seen in the form of discrepancies between different sets of published parameters, and temperature has generally not been taken into account. Finally, it must be remembered that the empirical bond valence-bond length relations will always be approximations, as exemplified by the different Ti-O bond lengths found with EXAFS for monomeric $Ti(OR)_4$ species with different R groups [7], where, according to the valence sum rule, all bonds should have unity valence.

Sometimes structures fail to obey the valence sum rule even with appropriate parameters and a correct model. This may be due to anisotropic electronic effects such as lone electron pairs, or due to steric constraints, preventing the atoms from rearranging in a better way. The asymmetry of the hydrogen bond is also a steric effect and application of the bond valence method is not straightforward. But even for "well-behaved" alkoxides, the method does not always succeed in predicting the location of missing protons: in the $Ln_3(O^tBu)_9(HO^tBu)_2$ structure published for Ln = Ce [36] in space group $P2_1$, two O^tBu groups have lower ligand BVS than expected (0.3 instead of 0.8-1.1) and are most probably protonated; in its $P2_1/c$ modification, reported for La, Y and Dy [37, 38, 14], on the other hand, one HO^tBu group could be assigned clearly, whereas several other ligands have only partially lowered BVS. In these cases, it seems that space group restrictions are responsible for the lack of differentiation in bond lengths.

In conclusion, the BVS method is a potentially powerful structure analysis method if properly used. Deviations from the expected valences can point to errors in the structural model such as erroneous oxidation states or even elements, or missing protons on ligands; they can point to electronic or steric effects, or even crystal packing restrictions, but quite frequently also simply to the lack of appropriate parameters. For the present studies, the bond valence parameters used for europium(III) and titanium(IV) [39] always lead to overestimated bond valence sums whereas bond valence sums for potassium(I) [39] tend to be underestimated. As already noted, future improvements are still to be expected.

The BVS method applied to alkoxides

Since there are no true bond valence parameters applicable to the carbon-oxygen bonds in alkoxides, one can only calculate total ligand BVS for the alkoxide groups OR, ignoring the information present in the C-O bond lengths. It can, however, be argued that bond valence and bond order should be the same, which would justify the use of parameters relating bond length to calculated bond order derived by Lendvay for single C-O bonds [40], allowing atomic BVS to be calculated for the O atoms. Two assumptions must then be made: 1) that bond valence and bond order are the same, and that in alkoxides, non-integer bond orders are subject to the same expression as in purely organic compounds for which the parameters were derived, and 2) that the C-O distances are reliable. C-O distances may not always be reliable enough, as seen in $Dy_3(O^tBu)_9(THF)_2$ [14] where the C-O bonds reported for the adducted THF molecules are so small that their oxygen atoms obtain BVS of as much as 2.6 instead of 2. In the analogous $Nd_3(O^tBu)_9(THF)_2$*2THF [41], all THF oxygen atoms instead have BVS of 1.7-1.9. Because of these uncertainties, this thesis will mainly report the total BVS for polyatomic ligands and only mention oxygen BVS values calculated using Lendvay's parameters as an additional check. BVS values for (hydr)oxo ligands are of course unaffected.

3. Results and discussion

3.1 Overview of compounds

Table 4 summarises the compounds and characterisations presented in papers I and II.

Table 4. Overview of compounds and experimental outcome

Paper	Compound	SCXRD	IR	UV-Vis
I	$Eu_3K_3TiO_2(OMe/OH)$-$(O^tBu)_{11}(HO^tBu)$ (**1**)	structure solved & refined	interpreted and consistent with crystal structure	*not measured*
II	$Eu_4TiO(O^iPr)_{14}$ (**2**)	structure solved & refined	consistent with $Ln_4TiO(O^iPr)_{14}$	consistent with crystal structure
II	$(Eu_{0.5}La_{0.5})_4Ti(O^iPr)_{14}$ (**3**)	structure solved & refined	consistent with $Ln_4TiO(O^iPr)_{14}$	consistent with crystal structure
II	$Eu_2Ti_4O_2(OEt)_{18}(HOEt)_2$ (**4**)	*not measured*	consistent with $Ln_2Ti_4O_2(OEt)_{18}(HOEt)_2$	consistent with assumed structure

3.2 Syntheses

In correspondence to literature, the metathesis route was successful for the synthesis of $Ln_4TiO(O^iPr)_{14}$ (equation 3.1) and $Ln_2Ti_4O_2(OEt)_{18}(HOEt)_2$. The introduction of Eu and La as halides at the same stage in the synthesis of $(Eu,La)_4TiO(O^iPr)_{14}$ allowed for thorough mixing and crystallisation of $(Eu_{0.5}La_{0.5})_4Ti(O^iPr)_{14}$ at the end of the synthesis.

Also reported in literature is the direct reaction between $Pr_5O(O^iPr)_{13}$ and $Ti(O^iPr)_{14}$ to give $Pr_4TiO(O^iPr)_{14}$. However, an attempt to prepare Eu_4TiO by mixing $Eu_5O(O^iPr)_{13}$ with $Ti(O^iPr)_4$ (in a cuvette, in order to follow the reaction with UV-Vis spectroscopy) failed, even after extended heating. The tentative equations 3.2 and 3.3 show one possible explanation: for four molecules of $Eu_5O(O^iPr)_{13}$, one additional oxo bridge needs to be formed, be it by elimination of ether (eq. 3.2) / other organic decomposition products, or by hydrolysis (eq. 3.3). Maybe hydrolysis is needed for this reaction to occur.

$$4\ EuCl_3 + 12\ KO^iPr + Ti(O^iPr)_4 + H_2O \rightarrow Eu_4TiO(O^iPr)_{14} + 12\ KCl_{(s)} + 2\ HOR \quad (3.1)$$

$$4\ Eu_5O(O^iPr)_{13} + 5\ Ti(O^iPr)_4 \rightarrow 5\ Eu_4TiO(O^iPr)_{14} + {}^iPr_2O \quad (3.2)$$

$$4\ Eu_5O(O^iPr)_{13} + 5\ Ti(O^iPr)_4 + H_2O \rightarrow 5\ Eu_4TiO(O^iPr)_{14} + 2\ HO^iPr \quad (3.3)$$

In contrast to the success of the metathesis route so far, metathesis attempts between $EuCl_3$ and K and Ti oxo-*tert*-butoxides failed to go to completion. After prolonged reaction time, and even after several days of heating at 60°C, the solutions would always contain potassium and less europium than expected. However, for the synthesis attempt with $K:Ti:Eu:H_2O$ = 6:1:2:1, the amount of europium in solution was at least increased significantly by the heating, and it was decided that the solution was to be centrifuged off the precipitate. Furthermore, since infrared spectra on the solution showed a superposition of the spectrum of $Ti(O^tBu)_4$ and that of unknown alkoxide(s), solvent replacement (from toluene:*tert*-butanol solvent to pure *tert*-butanol) was performed, with success in precipitating the unknown(s). Table 5 shows analysis results at different stages.

The *tert*-butanol supernatant, now enriched in $Ti(O^tBu)_4$, was removed and the white precipitate redissolved in excess toluene. The crystals growing over time from this solution were analysed by EDS, IR and X-ray diffraction and were shown to consist of $Eu_3K_3TiO_2$-$(OR)_{12}(HOR)$. Equations 3.4 and 3.5 allow for comparison between the targeted and obtained net reactions and show that the formation of $Eu_3K_3TiO_2(OR)_{12}(HOR)$ must have consumed all KOR in disfavour of the displacement by $EuCl_3$. Thus, this is one example of failure of the metathesis route: in order to obtain tert-butoxides of empirical formula $Eu_2TiO(OR)_8$ one may need to consider different synthesis paths.

Targeted reaction:

$$4\ EuCl_3 + 12\ KOR + 2\ Ti(OR)_4 + 2\ H_2O \rightarrow 2\ Eu_2TiO(OR)_8 + 12\ KCl_{(s)} + 4\ HOR \qquad (3.4)$$

Obtained reaction:

$$4\ EuCl_3 + 12\ KOR + 2\ Ti(OR)_4 + 2\ H_2O \rightarrow Eu_3K_3TiO_2(OR)_{12}(HOR) + EuCl_3 + Ti(OR)_4 + 9\ KCl_{(s)} + 3\ HOR \qquad (3.5)$$

Table 5. Analysis results at various stages of the synthesis of $Eu_3K_3TiO_2(OR)_{12}(HOR)$.

Analysis	Sample / stage	Result
Elemental analysis	Centrifuged liquid phase after room temperature	**Virtually no Eu**
Elemental analysis	Centrifugation sediments after room temperature	**Mainly Eu and Cl**
Elemental analysis	Centrifuged liquid phase after heating	**Eu:K:Ti ~ 2:4:1**
Elemental analysis	Centrifugation sediments after heating	**Eu, K and Cl**
Infrared spectroscopy	Centrifuged liquid phase after heating	*$Ti(O^tBu)_4$ + unknown(s)*
Infrared spectroscopy	HO^tBu supernatant after solvent replacement	*Mainly $Ti(O^tBu)_4$*
Infrared spectroscopy	White precipitate after solvent replacement	*No $Ti(O^tBu)_4$*
Elemental analysis	Crystals	**Eu:K:Ti ~3:3:1**

To further complicate matter, X-ray diffraction results show that one of the R groups is either a methyl group or a hydrogen atom in random distribution. The mechanism of formation of these groups was not studied, but it is most likely that the heat treatments have caused a decomposition of one *tert*-butoxo into a methoxo or hydroxo ligand. If decomposition of $OC(CH_3)_3$ into OCH_3 and OH as well as unknown byproducts has indeed occurred, this must have involved multiple C-C bond cleavages.

In fact, a synthesis attempt with stoichiometry Eu:K:Ti=3:12:1 (instead of 4:12:2) and reduced heating temperature yielded $Eu_3K_3TiO_2(OR)_{12}(HOR)$ only as a minor product, whereas the main product appears to be methoxide free as judged from IR spectroscopy. This has, however, not been confirmed by X-ray diffraction studies yet.

3.3 $Eu_3K_3TiO_2(OMe/OH)(O^tBu)_{11}(HO^tBu)$

The solid-state molecular structure of $Eu_3K_3TiO_2(OR)_{12}(HOR)$ (**1**) based on X-ray data is shown in figure 10. It is centered around an Eu_3K_3O octahedron and a K_3TiO tetrahedron, surrounded by 13 alkoxo ligands, bridging the metal ions as $[Eu_3K_3Ti(\mu_6\text{-}O)(\mu_4\text{-}O)](\mu_3\text{-}OR)_7(\mu_2\text{-}OR)_2(t\text{-}OR)$, i.e. one sextuply-bridging oxo ligand, one quadruply-bridging oxo ligand, seven triply bridging alkoxo ligands, two doubly bridging alkoxo ligands and one terminal alkoxo ligand.

For charge balance, the structure must contain an additional proton at one of the oxygen atoms. This cannot be found from x-ray diffraction data, but geometric considerations might reveal its location. BVS values were calculated for all ligands (excluding C-O contributions) as well as for all oxygen atoms (including C-O contributions). Only the μ_6-O ligand/atom has a much lower BVS than expected (1.4 instead of 2.0), whereas all other ligands/oxygen atoms have BVS close to the expected values (2 for oxygen atoms, and, without C-O contributions, 1 for OR ligands). The distribution of bond valences thus suggests that the μ_6-O ligand is in fact a μ_6-OH ligand. However, a strongly polarising H^+ inside the octahedron would either cause a distortion of the O atom in the direction of one of the faces of the octahedron, or cause high atomic displacement parameters for the O atom, if the hydrogen atom were statistically distributed over several energy minima. Yet, the μ_6-O atom is neatly centered in a rather regular octahedron and has low atomic displacement parameters. A comparison can be made with "$Ba_6O(moe)_{10}(moeH)_4$" [42], which also has an unidentified proton (only three out of four protons could be conclusively located on alkoxide ligands) as well as a BVS as low as 1.1 for the central oxo ligand; at the same time, it has crystallographic C_i symmetry, and the

last proton was concluded to be distributed over the alkoxo ligands. With the same type of argument, the last proton in the current complex is assumed to reside on one of the alkoxo ligands. The formula then becomes $Eu_3K_3TiO_2(OR)_{12}(HOR)$.

As already mentioned in 3.2, it also turned out that one of the R groups is in fact a methyl group, or rather a mixture of a methyl group and a hydrogen atom, as reflected by the low electron density found by Fourier refinement of the X-ray diffraction data. IR spectroscopy corroborates this picture of a methoxo group and an OH group present in the structure. Again, it is unlikely that the extra proton is on this ligand, and the chemical formula is therefore written $Eu_3K_3TiO_2(OMe/OH)(O^tBu)_{11}(HO^tBu)$.

IR spectroscopy shows support for this structural model. Table 6 shows our interpretations of selected peaks from the spectrum shown in figure 11.

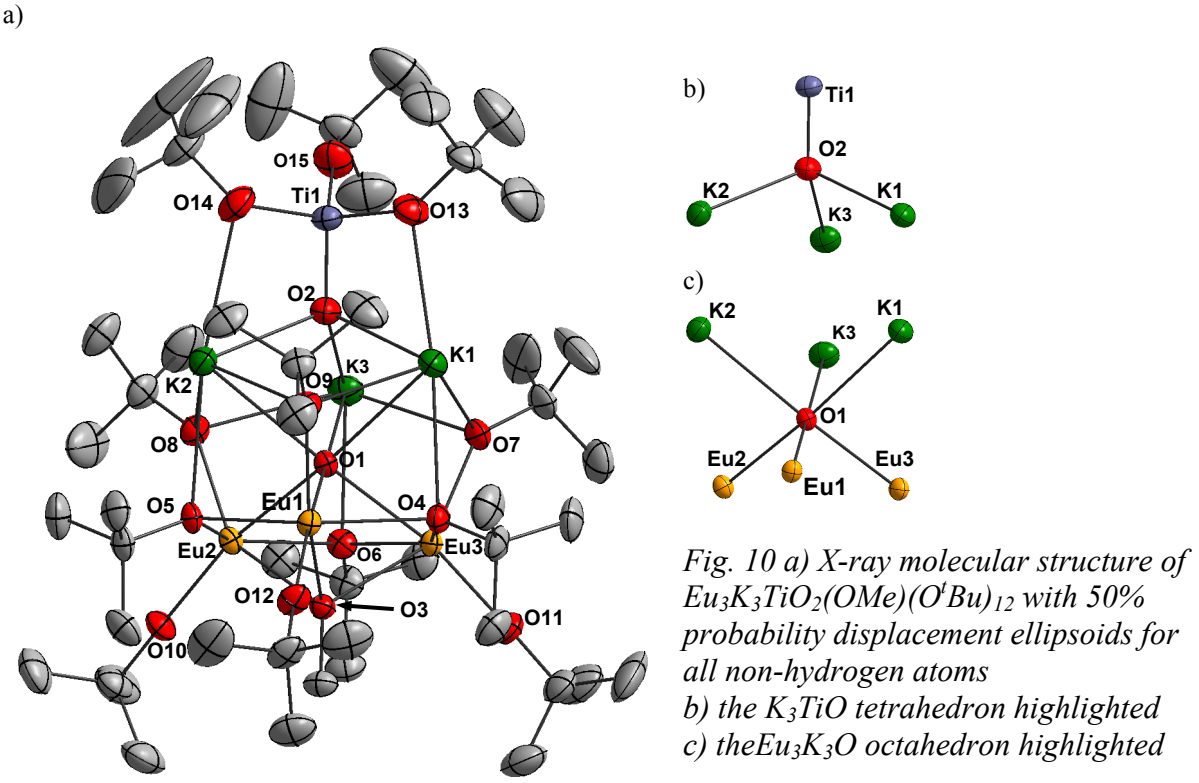

Fig. 10 a) X-ray molecular structure of $Eu_3K_3TiO_2(OMe)(O^tBu)_{12}$ with 50% probability displacement ellipsoids for all non-hydrogen atoms
b) the K_3TiO tetrahedron highlighted
c) theEu_3K_3O octahedron highlighted

In many ways, complex **1** has an interesting structure. The face-sharing of the Eu_3K_3O octahedron and the K_3TiO tetrahedron bears closest resemblance to the face-sharing of a Ba_6O octahedron and a Ba_3Li_3O prismoid in $Ba_6Li_3O_2(O^tBu)_{11}(THF)_3$ [43]. Both structures could be regarded as basically octahedral structures, to which $[Li_3(\mu_3\text{-}O^tBu)(t\text{-}O^tBu)_3]^-$ or $[Ti(O^tBu)_3]^+$ respectively was added in a form of self-assembly. The question then arises if there exist similar systems, where both the octahedron and the entity to be attached are bidirectional, enabling the self-assembly of linear polymers with interesting properties.

The molecular symmetry appears to include an internal mirror plane (through Eu1, K3, Ti1, O1, O2, O3, O9, O12 and O15), although this is strictly lost on crystallisation in space group $P2_1/n$. There is also a high tendency towards threefold rotation symmetry extending from the Eu side of the molecule to the three potassium atoms. Even the carbon atoms of the *tert*-butyl groups on O10-12 and O7-9 conform quite well to the threefold symmetry. The tetrahedron around O2, on the other hand, is distorted: only two of the three potassium atoms (K1 and K2) share bridging ligands (O13,O14) with the apical titanium atom. In the crystal structure, O15 forms no bond to K3, but one could imagine that in solution, O15 and K3 might occasionally come in contact, on breaking of the K1-O13 or K2-O14 bond, in a kind of

fluxional behaviour. In that case, the average molecular symmetry in solution would be C_{3v} and not C_s. The missing hydrogen atom could play part in such a mechanism.

Another interesting view on the structure arises from regarding the K^+ ions as being coordinated by two chelating complex ligands: $[Eu_3(\mu_3\text{-OMe})(\mu_3\text{-O})(\mu_2\text{-O}^t\text{Bu})_3(\text{t-O}^t\text{Bu})_6]^{(3-x)-}$ (left side in fig. 12) acting as a heptadentate ligand, its μ_3-O becoming μ_6-O, and three μ_2-O^tBu as well as three t-O^tBu becoming μ_3-O^tBu in **1**; and $[TiO(O^tBu)_3]^{x-}$ (right side in fig. 12) acting as a tridentate ligand with t-O becoming μ_4-O and two t-O^tBu becoming μ_2-O^tBu in **1**. The triangular Eu_3-based ligand can be compared with the $Ln_3(\mu_3\text{-O}^t\text{Bu})_2(\mu_2\text{-O}^t\text{Bu})_3(\text{t-H}_{0.33}\text{O}^t\text{Bu})_6$ structure (cf. figure 4e) reported for Ln=La/Y/Dy/Ce [37, 38, 14, 36], which also should exist for Eu, lying in between Dy and Ce in the 4f-lanthanoid series. The protonation of terminal ligands found for this triangular structure might even suggest that the unidentified proton in the present structure is on one of europium's terminal ligands.

Table 6. Selected IR bands/peaks

Broad band ~3400 cm^{-1}	OH-stretch in H-bonded alcohol
Very sharp peak at 3670 cm^{-1}	OH-stretch in free OH^-
Peaks around 1350 cm^{-1}	CH_3 umbrella modes
Peaks between 1210 and 1000 cm^{-1}	C-O and C-C stretching and bending
maximum at 1204 cm^{-1}	Tertiary alkoxide C-O peaks
maximum at 1050 cm^{-1}	Methoxide C-O peak
Peak at ~580 cm^{-1}	Ti-O stretching
Peaks between 550 and 360 cm^{-1}	Eu-O stretching

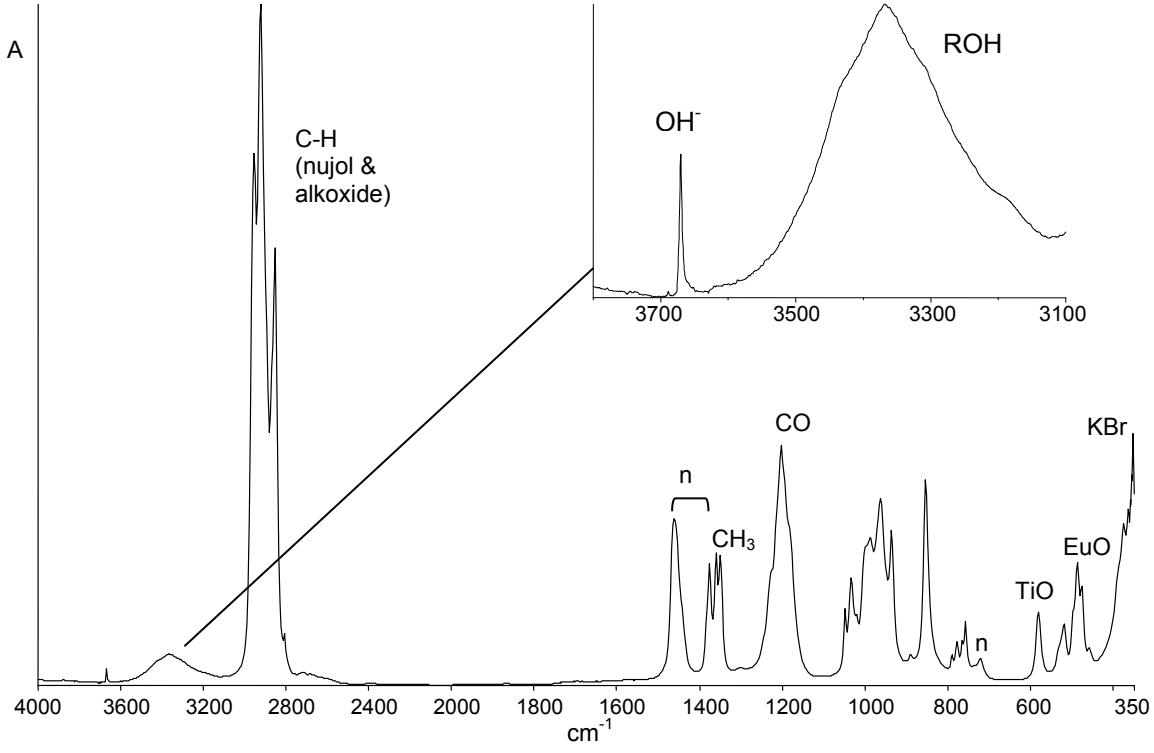

*Fig. 11 IR spectrum of **1** (n = peaks due to nujol)*

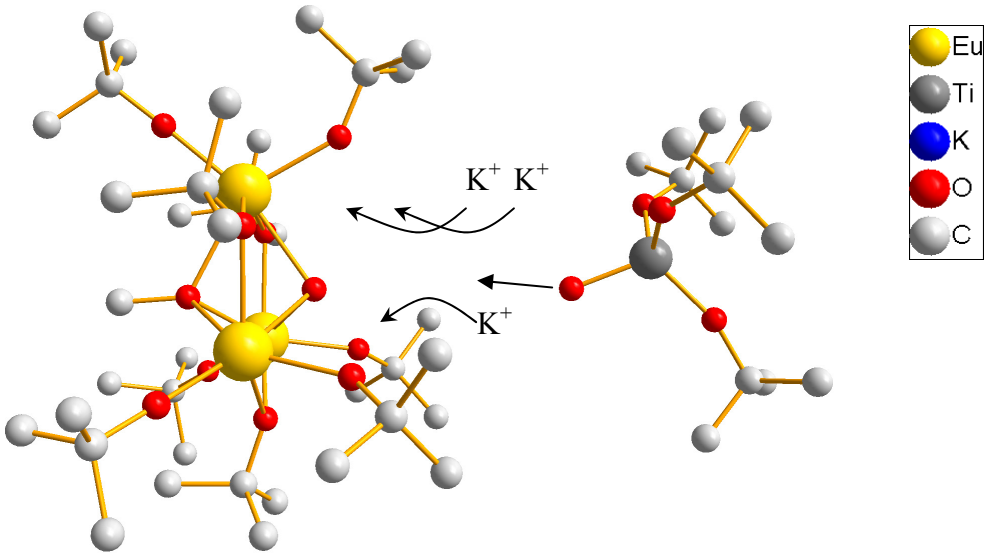

Fig. 12 $[Eu_3(\mu_3\text{-}O)(\mu_3\text{-}OMe)(\mu_2\text{-}O^tBu)_3(t\text{-}O^tBu)_6]^{(3-x)-}$, 3 K^+ and $[TiO(O^tBu)_3]^{x-}$ separated. x=0 corresponds to the unidentified proton being in the titanium part of the structure and x=1 corresponds to the unidentified proton being in the europium part of the structure.

3.4 $Eu_4TiO(O^iPr)_{14}$ and $(Eu_{0.5}La_{0.5})_4TiO(O^iPr)_{14}$

$Eu_4TiO(O^iPr)_{14}$ (**2**), and $(Eu_{0.5}La_{0.5})_4TiO(O^iPr)_{14}$ (**3**) crystallise in the same space group and with the same molecular structure as previously described for $Sm_4TiO(O^iPr)_{14}$ and $(Er_{0.1}Tb_{0.9})_4TiO(O^iPr)_{14}$ [24, 26]. The structure of **2** is shown in figure 13. With one μ_5-bridging oxo ligand (O8) and two μ_3-bridging, six μ_2-bridging and six terminal *iso*-propoxo ligands, the structural formula can be expanded to $Eu_4Ti(\mu_5\text{-}O)(\mu_3\text{-}O^iPr)_2(\mu_2\text{-}O^iPr)_6(t\text{-}O^iPr)_6$. The molecular symmetry is C_{2v}, but this is reduced to C_2 in the crystal structure.

The structure of **3** is very similar to that of **2**, both in the metal-oxygen framework and in the distribution of ligands, with similar angles and bond lengths as well as the appearance of positional disorder for the same two carbon atoms in both structures. This similarity goes to a further extent than the similarity to or between $Sm_4TiO(O^iPr)_{14}$ and $(Er_{0.1}Tb_{0.9})_4TiO(O^iPr)_{14}$, even when positional disorder is not included in the refinements.

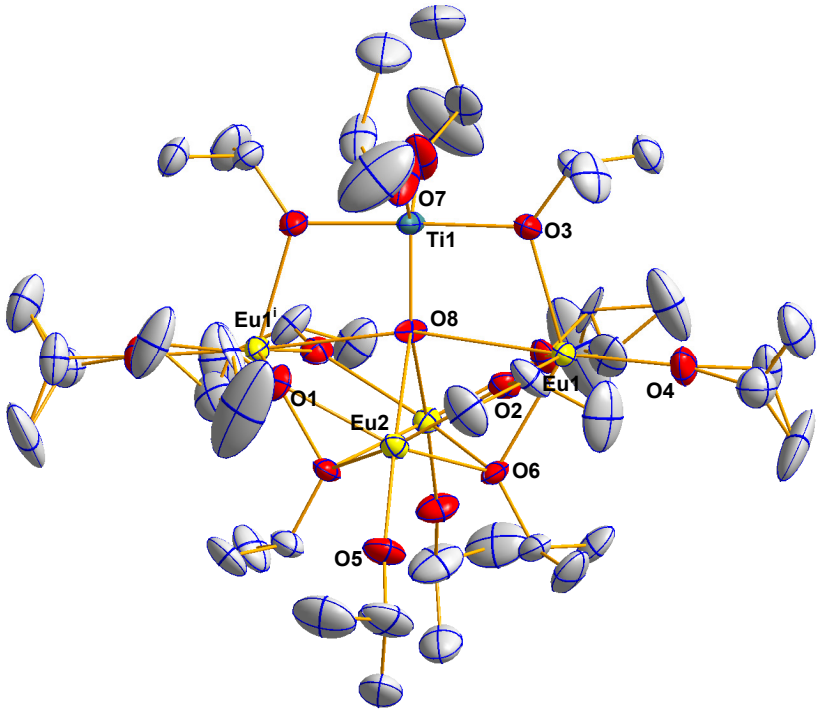

Fig. 13 Structure of $Eu_4TiO(O^iPr)_{14}$ with 50% probability displacement ellipsoids for all non-hydrogen atoms. Disorder of iso-propyl groups is shown on O1 and O4 in the form of multiple carbon atom sites.

Comparison of bond lengths for **2** (Ln=Eu) and **3** (Ln=$Eu_{0.5}La_{0.5}$) shows that Ln–O bond lengths are elongated by on average 1.6% on going from **2** to **3**, in agreement with the 3.4% larger ionic radius sum $r(Ln^{3+})+r(O^{2-})$ for La^{3+} compared to Eu^{3+}. Ln–O bond lengths in **3** are therefore unusually long for Eu^{3+} and unusually short for La^{3+}. Probably, the bond lengths in each single molecule are adapted to the actual Ln^{3+} ions within that specific molecule, but for the average molecule, the electron density corresponding to atomic positions is smeared out in space, as reflected by the atomic displacement factors being about 50% larger in **3** than in **2**. As expected, Ti–O, C–O and C–C bond lengths are not affected by the substitution.

Vibrational spectra for **2** and **3** can be compared with a vibrational spectrum that was previously recorded for $La_4TiO(O^iPr)_{14}$ [44] (fig. 14). This shows a smooth transition from $Eu_4TiO(O^iPr)_{14}$ to $La_4TiO(O^iPr)_{14}$ where some peaks gradually move and others gradually appear/disappear.

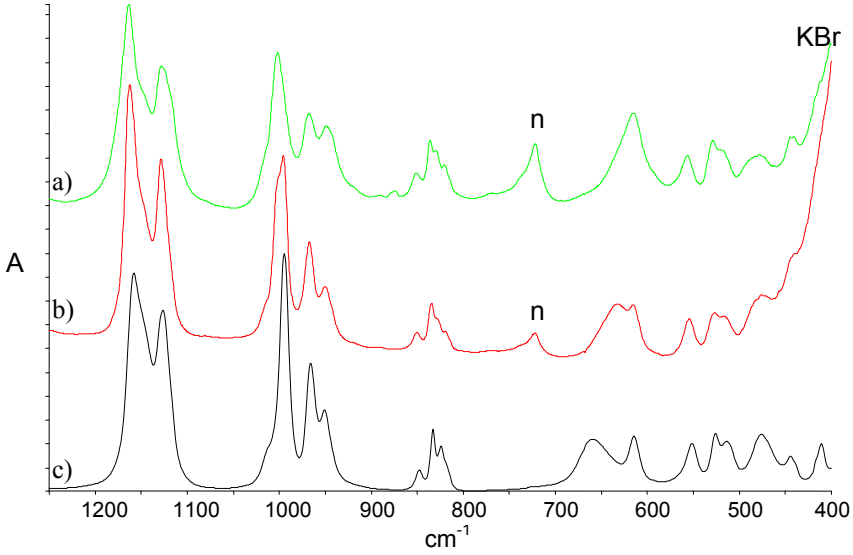

Fig. 14 IR spectra for a) $Eu_4TiO(O^iPr)_{14}$, b) $Eu_2La_2TiO(O^iPr)_{14}$, c) $La_4TiO(O^iPr)_{14}$ [44] (n = peaks due to nujol, KBr = absorption by the potassium bromide discs)

μ_5-O structures

The coordination of the central oxygen atom in **2** and **3** by four Eu atoms and one Ti atom can be described either as a distorted square pyramid with two of the basal corners bent downwards, or as a trigonal bipyramid with both Eu and Ti in equatorial position (figure 15).

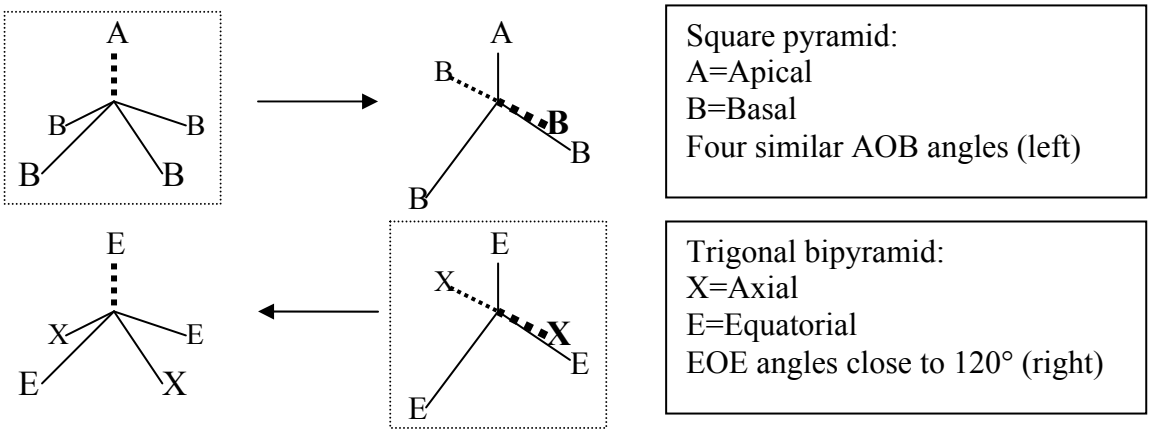

Figure 15. Fivefold coordination geometries around a central oxygen atom – square pyramid (B_4AO) and trigonal bipyramid (E_3X_2O) – and the relations between the two. Characteristics, as well as definitions of the different positions, are shown to the right.

With **2** and **3**, there are now four $Ln_4TiO(O^iPr)_{14}$ structures available for comparison with other Ln_4MO alkoxides where Ln is a trivalent lanthanoid and M is either Ln(III), Ti(IV) or Eu(II). Among the *iso*-propoxides, nine structures of formula $Ln_5O(O^iPr)_{13}$ have been published (Ln=Sc, Y, $Y_{0.8}Pr_{0.2}$, Nd, Eu, Gd, Er – two polymorphs, and Yb) [25, 45-50], with the same structure as the indium *iso*-propoxide $In_5O(O^iPr)_{13}$ [51]. In addition, a solvated neodymium *iso*-propoxide of formula $Nd_5O(O^iPr)_{13}(HO^iPr)_2$ was published [52], as well as the mixed-valence europium *iso*-propoxide $Eu_4Eu(II)O(O^iPr)_{12}(HO^iPr)$ [53]. A clear border can be drawn between on one hand $Ln_5O(O^iPr)_{13}$ and $Ln_4Eu(II)O(O^iPr)_{12}(HO^iPr)$ and on the other hand $Ln_5O(O^iPr)_{13}(HO^iPr)_2$ and $Ln_4TiO(O^iPr)_{14}$. Whereas the shape of the M_5O part of the former ten is almost square pyramidal (figure 15, table 7), the M_5O part of the latter five is closer to a trigonal bipyramid.

In the "square pyramidal" structures (fig. 16a), each basal LnO_6 octahedron shares faces with the apical LnO_6 octahedron and two of the other basal octahedra. In order for the basal octahedra opposite each other to come in face-sharing contact, they need to break their respective contacts to the apical octahedron apart from the common corner (μ_5-O). This is exactly what happens in the transformation of the "square pyramidal" to the "trigonal bipyramidal" structures (fig. 16b,c), which also allow for the "apical" M atom to have a coordination number of 5, as for M=Ti (fig. 16c). For M=Nd, the "trigonal bipyramidal" $Ln_5O(O^iPr)_{13}(HO^iPr)_2$ structure was crystallised at low temperature only [52], which reflects the lower thermal motion permitting the adduction of two solvent molecules.

Table 7. Parameters for square pyramidal and trigonal bipyramidal arrangements.

Structures	A-O-B angles	E-O-E angles	Geometry
Ln_5O..., $HLn_4Eu(II)O$...	very similar (93-97°)	dissimilar (up to 172°)	Square pyramidal
H_2Ln_5O..., Ln_4TiO...	differing at least 36°	rather similar (91-134°)	~Trig. bipyramidal

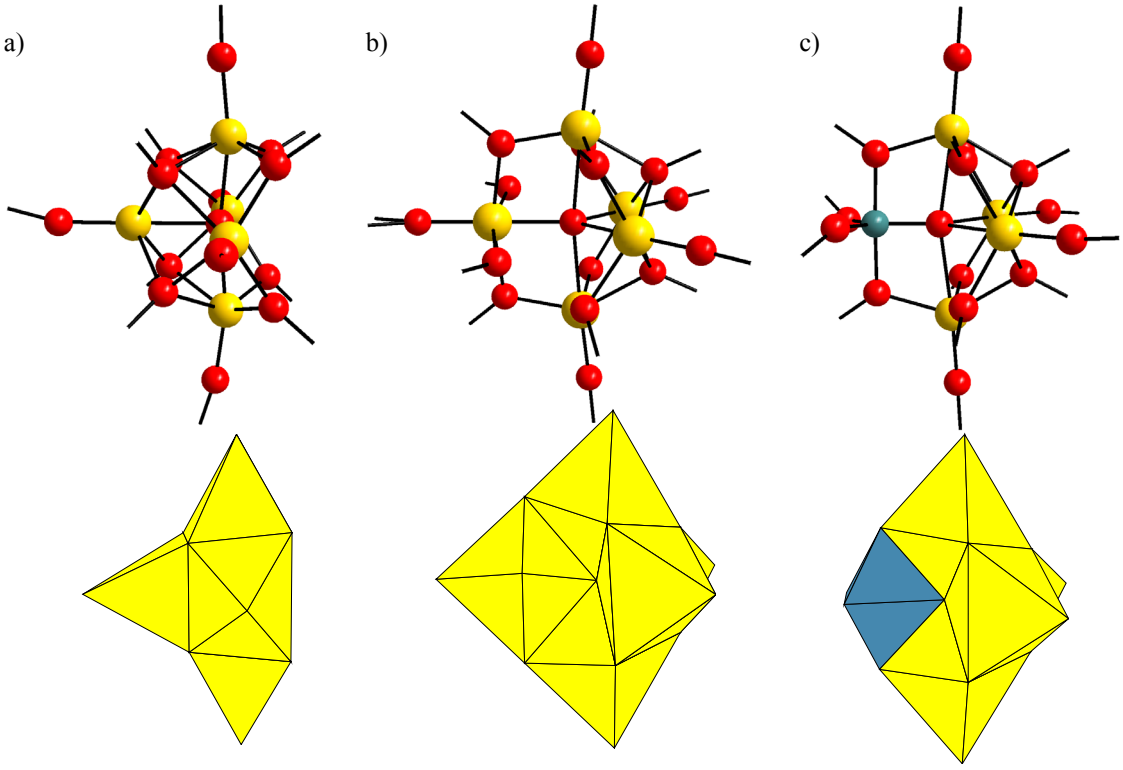

*Fig. 16 Ball-and-stick as well as MO_x polyhedron views of **a)** the $Ln_5O(O^iPr)_{13}$ structures with pyramidal arrangement of metal atoms around the central oxo ligand (a similar arrangement is found for $Ln_4Eu(II)O(O^iPr)_{12}(HO^iPr)$), **b)** the $Nd_5O(O^iPr)_{13}(HO^iPr)_2$ structure **c)** the $Ln_4TiO(O^iPr)_{14}$ structure with nearly trigonal bipyramidal arrangements.*

3.5 $Eu_2Ti_4O_2(OEt)_{18}(HOEt)_2$

The IR spectrum of the synthesised europium titanium oxo-ethoxide (fig. 17) matches that of $Er_2Ti_4O_2(OEt)_{18}(HOEt)_2$, indicating equal molecular structures.

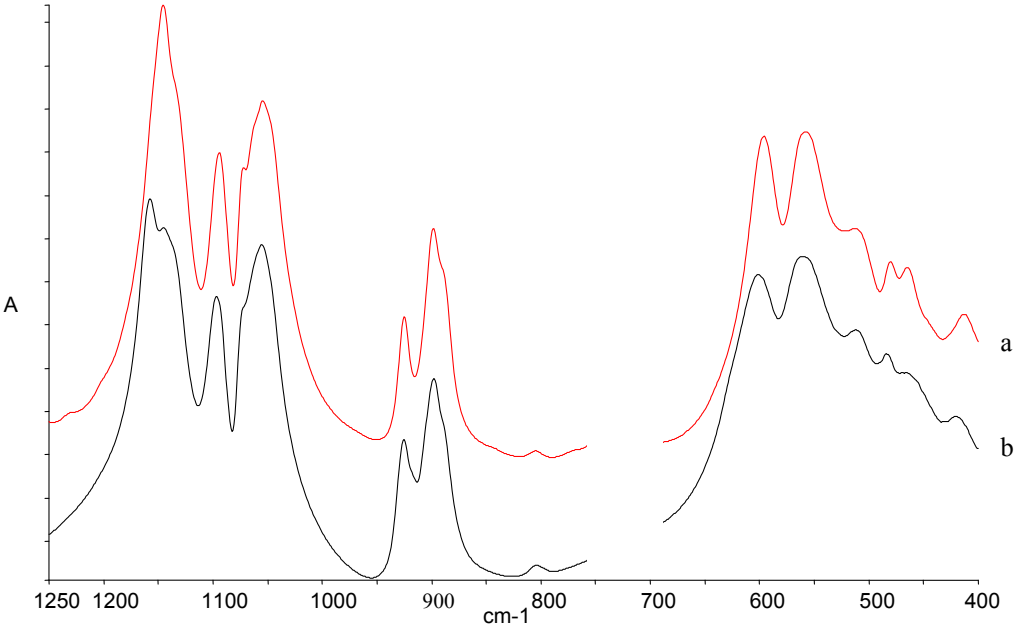

Fig. 17 IR absorption spectra of a) "$Eu_2Ti_4O_2(OEt)_{18}(HOEt)_2$" b) $Er_2Ti_4O_2(OEt)_{18}(HOEt)_2$

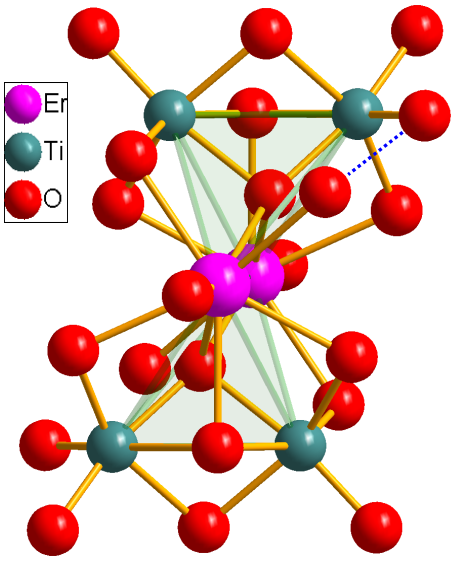

Fig. 18 Metal-oxygen structure of $Er_2Ti_4O_2(OEt)_{18}(HOEt)_2$. The dashed line is a hydrogen bond.

Fig. 18 shows the metal-oxygen part of the $Ln_2Ti_4O_2(OEt)_{18}(HOEt)_2$ molecular structure for Ln=Er. The molecules are centrosymmetric, and the two Ln atoms are equivalent. The structure contains two μ_4-bridging oxo ligands in severely distorted tetrahedral environments. In connection with this distortion, two hydrogen-bonded ligands EtOH...OEt on one side of the tetrahedron correspond to one OEt ligand on the other side.

The structure can be described in terms of triangular units $ErTi_2(\mu_3\text{-}O)(\mu_3\text{-}OEt)(\mu_2\text{-}OEt)_3(t\text{-}OEt)_5(t\text{-}HOEt)$ (cf. $LnTi_2(O^iPr)_9Cl_2$ [13], $Ln_3(O^tBu)_9(HO^tBu)_2$ [14, 36-38]). Fig. 19 shows how two such units may give $Er_2Ti_4(\mu_4\text{-}O)_2(\mu_3\text{-}OEt)_2(\mu_2\text{-}OEt)_8(t\text{-}OEt)_8(t\text{-}HOEt)_2$ through the attachment of Er to both the μ_3-O and one t-OEt ligand in the other unit, and of the alcoholic proton to another t-OEt ligand. The coordination number around Er^{3+} is raised from 6 in the triangular structures to 8.

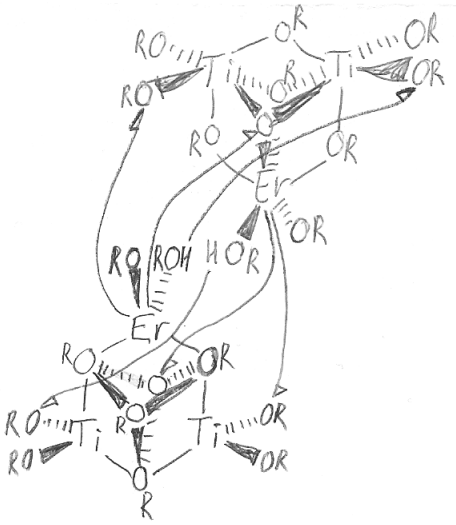

Fig. 19 Two "$ErTi_2(\mu_3\text{-}O)(\mu_3\text{-}OEt)(\mu_2\text{-}OEt)_3(t\text{-}OEt)_5(t\text{-}HOEt)$" units attaching mutually to each other, as described in the text

3.6 UV-Vis spectroscopy

The $Ln_4TiO(O^iPr)_{14}$ structure contains two distinct Ln^{3+} sites, whereas the $Ln_2Ti_4O_2(OEt)_{18}(HOEt)_2$ structure, with its inversion centre, only contains one unique Ln^{3+} environment. UV-Vis spectroscopy for Eu^{3+} confirms that two $^5D_0 \leftarrow {}^7F_0$ peaks are observed for $Eu_4TiO(O^iPr)_{14}$ and only one such peak is seen for $Eu_2Ti_4O_2(OEt)_{18}(HOEt)_2$ (figs. 20,21). For $(Eu,La)_4TiO(O^iPr)_{14}$, with randomly substituted La^{3+} for Eu^{3+}, the spectra look roughly the same as for $Eu_4TiO(O^iPr)_{14}$. If La^{3+} had taken only one specific site, one could have observed how one of the two $^5D_0 \leftarrow {}^7F_0$ peaks for Eu^{3+} would disappear, but unfortunately, the ions were too similar in size for site ordering to occur. The fine structure of the peaks is, however, slightly affected by the introduction of La^{3+} into the structure, as shown in fig. 22.

Comparison with the bipyramidal $Ln_5O(O^iPr)_{13}(HO^iPr)_2$ structure [52] would be interesting, since the main difference is the substitution of $Ln(t\text{-}HO^iPr)_2$ for $Ti(t\text{-}O^iPr)$, and such a comparison would show the effect of titanium on the $^5D_0$-$^7F_0$ energy separation. Unfortunately, at least in the case of Nd, this structure is not stable at room temperature, making UV-Vis measurements problematic.

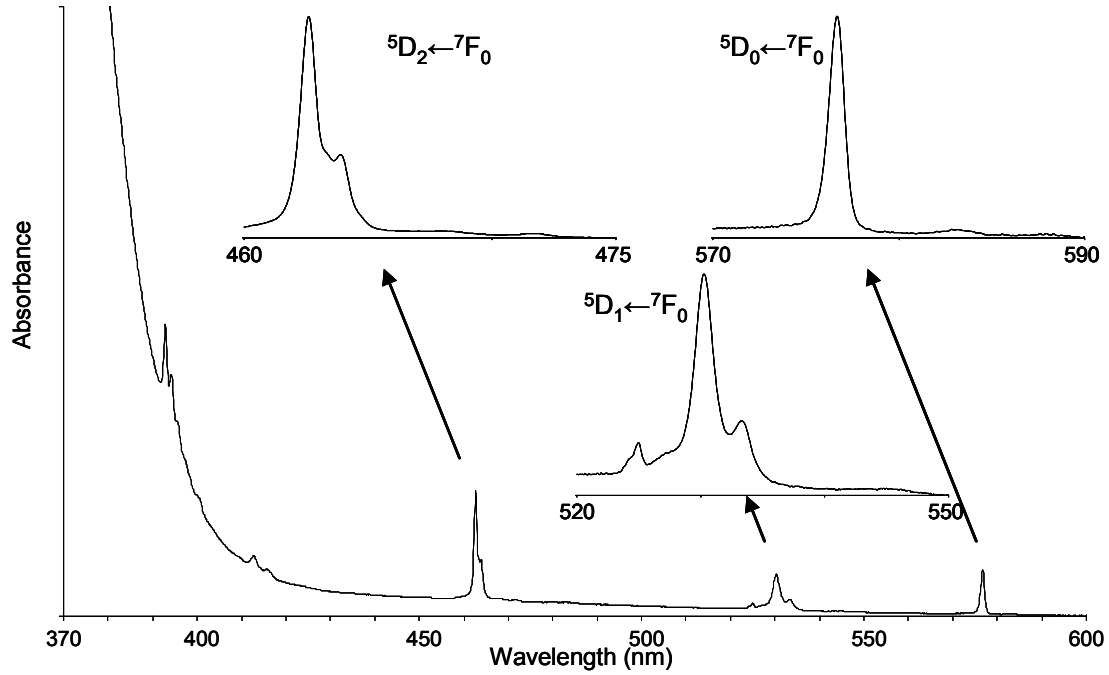

Fig. 20 Electronic absorption spectrum of $Eu_2Ti_4O_2(OEt)_{18}(HOEt)_2$

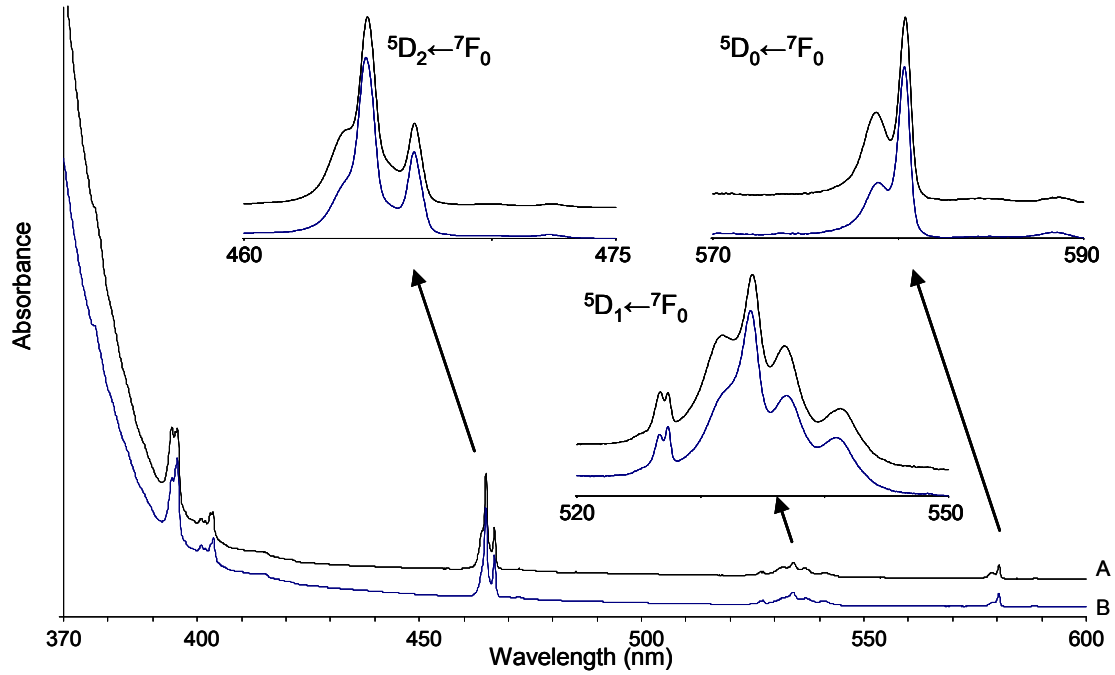

Fig. 21 Electronic absorption spectra of $Eu_4TiO(O^iPr)_{14}$ (A, upper curve) and $(Eu_{0.5}La_{0.5})_4TiO(O^iPr)_{14}$ (B, lower curve) as hexane solutions.

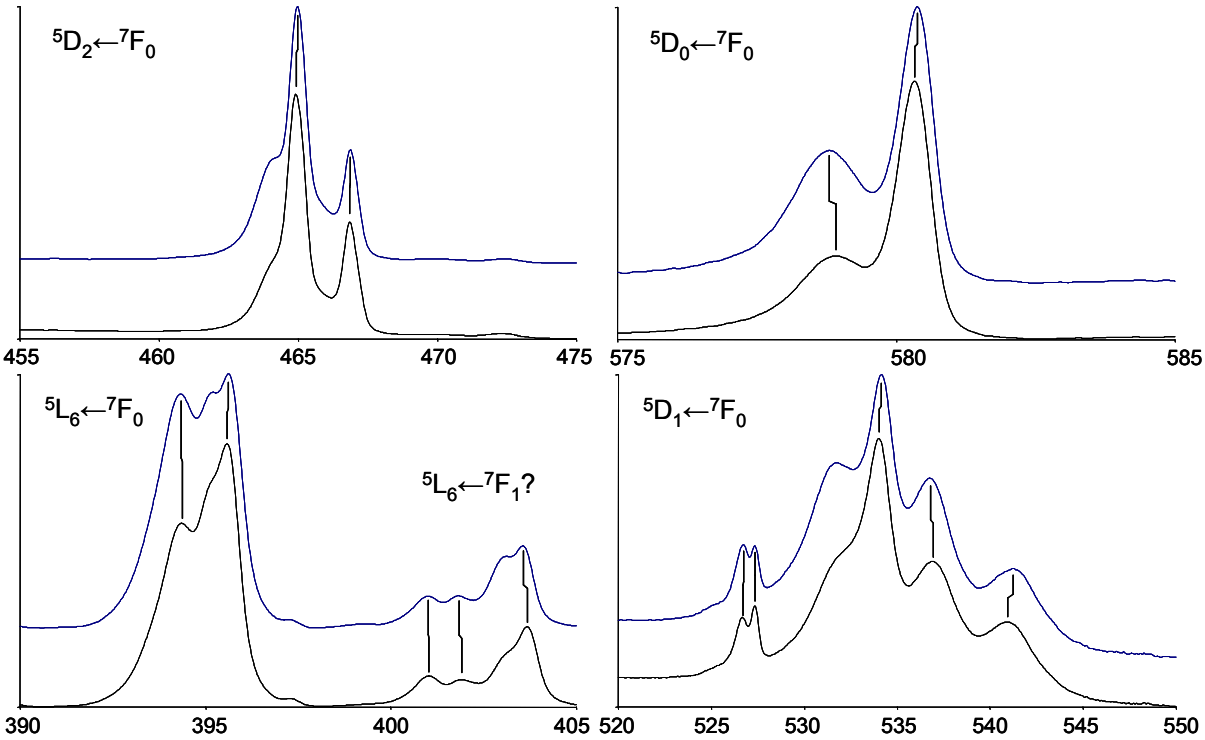

Fig. 22 Magnifications of selected peaks in figure y, showing the directions of the shifts (upper curves = $Eu_4TiO(O^iPr)_{14}$, lower curves = $(Eu,La)_4TiO(O^iPr)_{14}$).

4. Concluding remarks

1) A new heterotermetallic K-Ln-Ti oxo-alkoxide structure of formula $Eu_3K_3TiO_2(OMe/OH)$-$(O^tBu)_{11}(HO^tBu)$ has been obtained and described, mainly contributing with interesting information concerning the structures of lanthanoid alkoxides.

a) It provides one of few examples of lanthanoid-containing oxoalkoxides with μ_6-bridging oxo ligands. As in all other reported cases, the six-coordinated oxygen atom is surrounded partially by electropositive alkali metal atoms.

b) The inclusion of potassium to give this termetallic complex may be a factor standing in the way for a successful synthesis of europium titanium (oxo-)*tert*-butoxides by the metathesis route. But the low solubility/reactivity of $EuCl_3$ in the sterically hindered *tert*-butyl alcohol may also have played a part. Preliminary metathesis attempts with Na yielded neither europium-titanium or termetallic Na-Er-Ti complexes. In order to obtain europium titanium *tert*-butoxides, it thus seems that one needs to consider alternative synthesis routes.

c) Heating may have caused the decomposition of *tert*-butyl oxide ligands into methyl oxide and hydroxide ligands. The mechanism is unclear, but must seemingly have involved multiple C-C bond cleavages.

d) Like a few other oxoalkoxides, the obtained compound contains a proton which cannot conclusively be placed on any of the ligands. Geometric and crystallographic considerations speak against its placement on one of the oxo ligands, but there is also no clear indication to point out a specific alkoxide ligand as being protonated. It might be interesting to synthesise $Eu_3(O^tBu)_9(HO^tBu)_2$ as well as trying to replace one or two *tert*-butoxo groups with methoxo groups.

e) The structure contains face-sharing M_6O and M_4O polyhedra, which is unprecedented among reported related structures. The attachment of the titanium-centered group on top of the Eu_3OK_3 octahedron could be regarded as an example of self-assembly, and the question arises whether this insight can be used to design related structures for nano-engineering, if, e.g., two- or three-dimensional chains can be made by the same principles.

f) The structure and composition match no known target oxide for sol-gel synthesis. However, interestingly, the preparation of an intercalation compound of stoichiometry $K_2La_2Ti_3O_{10}$ was reported to involve an excess of K_2CO_3 to compensate for loss due to volatilisation [54]. $K_2La_2Ti_3O_{10}$ serves in turn as an intercalation precursor for a whole series of phases [55] which were subsequently shown to be promising as photocatalysts for water decomposition [56]. The alkoxide structure described in paper I fixes the ratio of K to Ln and would only require additional titanium alkoxide to lead to the proper stoichiometry, but whether the said compound will form, remains to be demonstrated.

2) The $Ln_4TiO(O^iPr)_{14}$ and $Ln_2Ti_4O_2(OEt)_{18}(HOEt)_2$ structures were reproduced for Ln=Eu. Also, the mixed-metal alkoxide $(La,Eu)_4TiO(O^iPr)_{14}$ was synthesised and characterised.

a) The $Ln_4TiO(O^iPr)_{14}$ structure is part of a larger group of Ln_4M oxo-alkoxides, and the prepared structures provide additional information for the comparison between Ln_4M structures with different identities of Ln and M.

b) The size difference between La^{3+} and Eu^{3+} is not enough for site-selective substitution in $Ln_4TiO(O^iPr)_{14}$. As a consequence, the experiments did not succeed in making one of two Eu^{3+} $^5D_0 \leftarrow {}^7F_0$ electronic absorption peaks disappear. However, Sc^{3+} and Er^{3+} have previously been shown to have sufficient size difference for at least partial site selectivity. With a still larger size difference between Sc^{3+} and Eu^{3+}, the substitution of Sc^{3+} for Eu^{3+} looks more promising than the currently investigated substitution. This combination would also provide a large difference in scattering power, facilitating their separation in structure determinations.

3) A new set of bond valence parameters might be useful for the field of lanthanoid alkoxides. A careful investigation using scrutinised data may also yield information as to how the different ligands affect bond lengths and geometries. An improved, parametrised model, may then better reveal the cases where sterical strain or ligand-ligand interactions cause deviations from the expected values.

Acknowledgements

First of all, I would like to thank my supervisor, Prof. Gunnar Westin, for convincing me that alkoxides are not exotic, scary organics, but rather coordination compounds no less inorganic than oxalates or acetates, and with interesting structures. I am grateful to him for giving me this opportunity to practise research in the field of lanthanoid alkoxides and of structure determination, and I will never regret having started these studies.

The rest of the "sol-gel" research group are also thanked for help and advice at various occasions.

The technical and administrative staff of the department, as well as the people responsible for various research equipment, are thanked for making all sorts of things work. Special thanks related to this specific work go to Associate prof. Torbjörn Gustafsson and Håkan Rundlöf for help with single-crystal diffraction practice and theory.

I am indebted to Prof. Jan-Otto Carlsson, Prof. Yvonne Brandt Andersson and director of research studies Prof. Leif Nyholm for investing time and trust in me for the completion of this thesis. My wife, Susanne, is also thanked for enduring the hard times and uncertainty, and for supporting me in my accomplishments.

I am also grateful to Prof. Rolf Berger, Dr. Annika Pohl and Prof. Gunnar Westin for having scrutinised this thesis in its later versions.

References

1. C.D. Chandler, C. Roger, M.J. Hampden-Smith, *Chem. Rev.* **93** (1993) 1205-1241.

2. U. Schubert, N.Hüsing, *Synthesis of Inorganic Materials, 2nd ed.*, Wiley-VCH, Weinheim (Germany) (2005).

3. L.L. Hench, J.K. West, *Chem. Rev.* **90** (1990) 33-72.

4. J. Livage, C. Sanchez, *J. Non-Cryst. Solids* **145** (1992) 11-19.

5. K.G. Caulton, L.G. Hubert-Pfalzgraf, *Chem. Rev.* **90** (1990) 969-995.

6. D.C. Bradley, *Chem. Rev.* **89** (1989) 1317-1322.

7. F. Babonneau, S. Doeuff, A. Leaustic, C. Sanchez, C. Cartier, M. Verdaguer, *Inorg. Chem.* **27** (1988) 3166-3172.

8. J.A. Ibers, *Nature* **197** (1963) 686.

9. K.J. Nelson, I.A. Guzei, G.S. Lund, R.W. McGaff, *Polyhedron* **21** (2002) 2017-2020.

10. P. Toledano, F. Ribot, C. Sanchez, *Acta Cryst.* **C46** (1990) 46.

11. B.A. Vaartstra, J.C. Huffman, P.S. Gradeff, L.G. Hubert-Pfalzgraf, J.-C. Daran, S. Parraud, K. Yunlu, K.G. Caulton, *Inorg. Chem.* **29** (1990) 3126-3131.

12. A. Senouci, M. Yaakoub, C. Huguenard, M. Henry, *J. Mater. Chem.* **14** (2004) 3215-3230.
13. M. Veith, S. Mathur, V. Huch, *Inorg. Chem.* **36** (1997) 2391-2399.
14. T.J. Boyle, S.D. Bunge, P.G. Clem, J. Richardson, J.T. Dawley, L.A.M. Ottley, M.A. Rodriguez, B.A. Tuttle, G.R. Avilucea, R.G. Tissot, *Inorg. Chem.* **44** (2005) 1588-1600.
15. T. Jüstel, H. Nikol, C. Ronda, *Angew. Chem.* **110** (1998) 3250-3271; *Angew. Chem. Int. Ed.* **37** (1998) 3084-3103.
16. J.-M. Breteau, *Proceedings of SPIE (International Society for Optical Engineering)* **2498** (1995) 154-163.
17. R.M. Petoral, F. Söderlind, A. Klasson, A. Suska, M.A. Fortin, N. Abrikossova, L. Selegård, P.-O. Käll, M. Engström, K. Uvdal, *J. Phys. Chem.* **C113** (2009) 6913-6920.
18. G. Westin, Å. Ekstrand, E. Zangellini, L. Börjesson, *J. Phys. Chem. Solids* **61** (2000) 67-74.
19. L.G. Westin, M. Kritikos, A. Caneschi, *Chem. Commun.* (2003) 1012-1013.
20. J. Gromada, A. Mortreux, T. Chenal, J.W. Ziller, F. Leising, J.-F. Carpentier, *Chem. Eur. J.* **8** (2002) 3773.
21. T.J. Boyle, L.A.M. Ottley, *Chem. Rev.* **108(6)** (2008) 1896-1917.
22. G. Westin, R. Norrestam, M. Nygren, M. Wijk, *J. Solid State Chem.* **135** (1998) 149-158.
23. G. Westin, M. Wijk, M. Moustiakimov, M. Kritikos, *J. Sol-Gel Sci. Tech.* **13** (1998) 125-128.
24. S. Daniele, L.G. Hubert-Pfalzgraf, J.-C. Daran, S. Halut, *Polyhedron* **13** (1994) 927-932.
25. L.G. Hubert-Pfalzgraf, S. Daniele, A. Bennaceur, J.-C. Daran, J. Vaissermann, *Polyhedron* **16(7)** (1997) 1223-1234.
26. M. Moustiakimov, M. Kritikos, G. Westin, *Acta Cryst.* **C54** (1998) 29-31.
27. M. Moustiakimov, *Ph.D. Thesis*, Stockholm University (2002).
28. R.C. Mehrotra, A. Singh, U.M. Tripathi, *Chem. Rev.* **91** (1991) 1287-1303.
29. A.F. Holleman, E. Wiberg, N. Wiberg, *Lehrbuch der Anorganischen Chemie, 101. Auflage*, Walter de Gruyter, Berlin (1995) – or A.F. Holleman, E. Wiberg, N. Wiberg, *Inorganic Chemistry, 101st ed.*, Walter de Gruyter, Berlin (2001).
30. K.B. Yatsimirskii, K.N. Davidenko, *Coord. Chem. Rev.* **27** (1979) 223-273.
31. K. Binnemans, C. Görller-Walrand, *Chem. Phys. Letters* **235** (1995) 163-174.
32. K. Binnemans, C. Görller-Walrand, *Chem. Phys. Letters* **245** (1995) 75-78.
33. I.D. Brown, *Chem. Rev.* **109** (2009) 6858-6919.
34. F.H. Allen, *Acta Cryst.* **B58** (2002) 380-388.
35. U. Müller, *Anorganische Strukturchemie, 4. Auflage*, Teubner Verlag, Wiesbaden (2004) – or U. Müller, *Inorganic Structural Chemistry, 2nd ed.*, John Wiley & Sons, Chichester (UK) (2006).
36. T.J. Boyle, L.J. Tribby, S.D. Bunge, *Eur.J.Inorg.Chem.* (2006) 4553.

37. D.C.Bradley, H.Chudzynska, M.B.Hursthouse, M.Motevalli, *Polyhedron* **10** (1991), 1049.
38. M.Veith, S.Mathur, A.Kareiva, M.Jilavi, M.Zimmer, V.Huch, *J.Mater.Chem.* **9** (1999) 3069.
39. N.E. Brese, M. O'Keeffe, *Acta Cryst.* **B47** (1991) 192-197.
40. G. Lendvay, *J. Mol. Struct. (Theochem)* **501-502** (2000) 389-393.
41. J.Gromada, T.Chenal, A.Mortreux, J.W.Ziller, F.Leising, J.-F.Carpentier, *Chem. Commun.* (2000) 2183.
42. K.G.Caulton, M.H.Chisholm, S.R.Drake, J.C.Huffman, *J. Chem. Soc., Chem. Commun.* (1990) 1498.
43. H. Bock, T. Hauck, C. Näther, N. Rösch, M. Staufer, O.D. Häberlen, *Angew. Chem.* (1995) 107:1439.
44. G. Westin, *private communication*.
45. E.P.Turevskaya, A.I.Belokon, Z.A.Starikova, A.I.Yanovsky, E.N.Kiruschenkov, N.Ya.Turova, *Polyhedron* **19** (2000) 705.
46. O.Poncelet, W.J.Sartain, L.G.Hubert-Pfalzgraf, K.Folting, K.G.Caulton, *Inorg.Chem.* **28** (1989) 263.
47. M.Kritikos, M.Moustiakimov, M.Wijk, G.Westin, *J.Chem.Soc.,Dalton Trans.* (2001) 1931.
48. G.Westin, M.Moustiakimov, M.Kritikos, *Inorg. Chem.* **41** (2002) 3249.
49. G.Westin, M.Kritikos, M.Wijk, *J.Solid State Chem.* **141** (1998) 168.
50. D.C.Bradley, H.Chudzynska, D.M.Frigo, M.E.Hammond, M.B.Hursthouse, M.A.Mazid, *Polyhedron* **9** (1990) 719.
51. D.C.Bradley, H.Chudzynska, D.M.Frigo, M.B.Hursthouse, M.A.Mazid, *J. Chem. Soc., Chem. Commun.* (1988) 1258.
52. G.Helgesson, S.Jagner, O.Poncelet, L.G.Hubert-Pfalzgraf, *Polyhedron* **10** (1991) 1559.
53. M.Moustiakimov, M.Kritikos, G.Westin, *Inorg. Chem.* **44** (2005) 1499.
54. J. Gopalakrishnan, V. Bhat, *Inorg. Chem.* **26** (1987) 4329-4301.
55. J. Gopalakrishnan, *Chem. Mater.* **7** (1995) 1265-1275.
56. T. Takata, Y. Furimi, K. Shinohara, A. Tanaka, M. Hara, J.N. Kondo, K. Domen, *Chem. Mater.* **9** (1997) 1063-1064.

Populärvetenskaplig sammanfattning på svenska

Bakgrund

Vårt moderna samhälle genomsyras av allehanda tekniska prylar. Dessa innehåller ett stort antal material med olika funktioner, t.ex. elektrisk ledning, magnetisk datalagring, synliggörande av information på skärmar. För de allra flesta av dessa material gäller att de måste framställas med avancerade metoder, och det finns olika tillvägagångssätt för olika material. Ett sätt är att utgå från molekyler i lösning. Sådan lösningsbaserad materialframställning kräver i allmänhet ganska mycket utvecklingsarbete och ibland även dyra kemikalier, men bland fördelarna kan nämnas minskat behov av värmebehandling och god kontroll över renhet och struktur i slutmaterialet, särskilt för material med komplicerad sammansättning (t.ex., $La_{0.75}Ba_{0.125}Sr_{0.125}MnO_3$, ett potentiellt framtida datalagringsmaterial).

Koordinationskomplex med alkoxidjoner

Koordinationskomplex kallas de kemiska föreningar där en centralatom omges av andra atomer eller atomgrupper som med sina elektroner skapar kemiska bindningar till centralatomen. Dessa atomgrupper som bidrar med elektroner kallas ligander. En av de vanligaste liganderna är vattenmolekylen, H_2O: om t.ex. koksalt (NaCl) löses i vatten, omges de små, positivt laddade natriumjonerna (Na^+) av ett antal vattenmolekyler för att bilda koordinationskomplex som $[Na(H_2O)_6]^+$. Hydroxidjonen (OH^-) är en annan vanlig ligand i vattenlösningar.

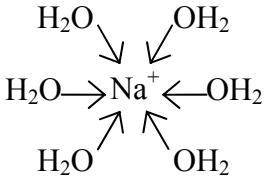

Fig. 1 Exempel på koordinationskomplex

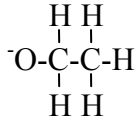

Fig. 2 Exempel på en alkoxidjon

Alkoxidjoner är ett slags ligander som kan finnas i organiska lösningsmedel. Man kan föreställa sig deras uppbyggnad som hydroxidjoner (OH^-) där väteatomen H bytts ut mot en kolvätegrupp, t.ex. CH_3 eller CH_2CH_3. I stället för att skriva hela formeln på kolvätekedjan, skriver man ofta ett R som allmän beteckning för en kolvätekedja, och den allmänna formeln för en alkoxidjon blir då OR^-.

Kolvätekedjan R i en alkoxidjon kan vara såväl kort som lång och kan vara enkel eller förgrenad. Denna variationsmöjlighet skapar även en variation i struktur hos koordinationskomplex där alkoxidjoner binder till metalljoner, och det är intressant att studera hur strukturerna påverkas av kolvätekedjans natur. Förgreningar tar t.ex. mer plats och kan därmed ställa geometriska krav på strukturen. Förutom att detta är intressant ur grundforskningssynpunkt, så är kunskap om strukturerna hos alkoxidkomplex även viktig i lösningsbaserad materialframställning, där de utgör vanliga utgångsämnen.

Alkoxidbaserad materialsyntes och oxo-alkoxider

Alkoxidjoner är starka baser, dvs de binder gärna till metalljoner för att bilda koordinationskomplex, men om de har chansen binder de allra helst till vätejoner för att bilda alkoholer, ROH (t.ex. CH_3CH_2OH). Denna chans får de bland annat om vattenmolekyler (H_2O, som även kan skrivas H–OH) finns närvarande, som då avger en vätejon till alkoxidliganden medan resten (OH) tar över rollen som ligand i koordinationskomplexen:

...M–OR + H–OH → ...M–OH + H–OR.

Även det komplex ...M-OH som bildats i ovanstående reaktion kan avge sin vätejon till alkoxidligander och byta plats med dessa i koordinationskomplex ...M*-OR:

...M*–OR + H–O–M... → ...M*–O–M... + H–OR

På så vis har två metallatomer M* och M kopplats ihop med en syrebrygga, och det är processer som denna som ligger till grund för materialframställning baserad på alkoxider i lösning. Alkoholerna H–OR som bildas avdunstar lätt, och om man fortsätter med att ersätta fler och fler alkoxidligander med syrebryggor har man till slut uppnått en ren metalloxid.

Syrejonerna O^{2-} som länkar samman metallatomerna kallas även oxoligander, och de molekylära komplex som innehåller både oxo- och alkoxidligander kallas oxo-alkoxider. Dessa komplex, som enligt ovan bildats genom sammankoppling av alkoxider, kan sägas vara ett steg i riktning mot fasta metalloxidmaterial, som oftast är slutmålet med alkoxidbaserad materialsyntes. Därför är oxo-alkoxidernas strukturer ännu viktigare än alkoxidernas strukturer för förståelsen och optimeringen av alkoxidbaserad materialsyntes.

Överhuvudtaget har oxo-alkoxider intressanta strukturer. Ofta är syreatomerna centralt placerade i molekylerna och binder till fler än två metallatomer, där geometrin och antalet omgivande metallatomer beror på både metallatomerna och alkoxidliganderna. Än återstår det det mycket att utforska, men en förhoppning är att man med växande kunskap om befintliga strukturer så småningom kan förutsäga nya molekylstrukturer som lämpar sig för syntes av nya material.

Studier av europium-titan-oxo-alkoxider

I denna avhandling ligger fokus på oxo-alkoxider av trevärt europium (Eu) och fyrvärt titan (Ti). I och med att alkoxider och oxo-alkoxider är känsliga för vatten, måste de framställas i inert atmosfär, t.ex. argon, utan lufttillträde. Alla reaktanter och lösningsmedel befinner sig då i en så kallad handskbox: för att hantera dessa trär man in händerna genom boxens handskar, som når in i den argonfyllda delen, där man kan verkställa reaktionerna.

Alla komplex har undersökts med infraröd-absorptionsspektroskopi, där topparna anger vilka atomgrupper och bindningar som finns i molekylerna (metylgrupp, etylgrupp, vätebindning osv.).

Några av komplexen har undersökts med absorptionsspektroskopi i synligt ljus, där särskilt en av topparna är lätt att tolka. Antalet gånger som denna test-topp förekommer motsvarar nämligen antalet europiumatomer i molekylen, eller rättare sagt: antalet europiumatomer med olika arrangemang av omgivande ligander.

Några komplex har även undersökts med enkristall-röntgendiffraktion, som kan ge de exakta atompositionerna i molekylerna (molekylstrukturen) när molekylerna har ordnat sig i kristaller. Molekylstrukturen i kristallerna är inte nödvändigtvis samma som molekyl-strukturen i lösning, men vanligtvis är de lika för denna typ av komplex och detta går att bekräfta med de spektroskopiska teknikerna.

Elementsammansättningen hos proverna har bestämts med hjälp av ett elektronmikroskop.

$Eu_2Ti_4O_2(OEt)_{18}(HOEt)_2$

Med etoxidjon ($^-$OEt = $^-OCH_2CH_3$, fig. 2) som ligand har $Eu_2Ti_4O_2(OEt)_{18}(HOEt)_2$ framställts. Av spektroskopiska data att döma har den samma molekylstruktur som erbium-titan-oxo-etoxiden $Er_2Ti_4O_2(OEt)_{18}(HOEt)_2$, fast med europium i stället för erbium. Molekylerna innehåller två syreatomer som koordinerar fyra metallatomer var: två europium- och två titanatomer. Molekylens två europiumatomer har exakt lika omgivning pga molekylens symmetri. Detta syns i absorptionen av synligt ljus, där den tidigare nämnda test-toppen visar på endast en sorts europiumatom.

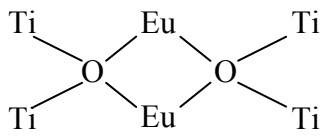

Fig. 3 Omgivningen runt de två oxoliganderna i $Eu_2Ti_4O_2(OEt)_{18}(HOEt)_2$

$Eu_4TiO(O^iPr)_{14}$ och $Eu_2La_2TiO(O^iPr)_{14}$

Med isopropoxidjon ($^-O^iPr$ = $^-OCH(CH_3)_2$) som ligand har $Eu_4TiO(O^iPr)_{14}$ framställts. Analys av data från spektroskopi och röntgendiffraktion visar att strukturen är densamma som samarium-titan-oxo-isopropoxiden $Sm_4TiO(O^iPr)_{14}$, med europium i stället för samarium. Varje molekyl innehåller en central syreatom som koordinerar alla fem metallatomer. De fyra europiumatomerna går att dela in i två grupper med olika omgivning. Detta bekräftas med spektroskopi i synligt ljus, där test-toppen är dubbel.

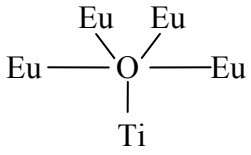

Fig. 4 Omgivningen runt oxoliganden i $Eu_4TiO(O^iPr)_{14}$

De två spektroskopiska topparna har olika våglängd och även något olika utseende, och det skulle vara intressant att kunna avgöra vilken topp som hör till vilken europiumplats. Ett försök gjordes att byta ut hälften av alla europiumatomer mot lantanatomer, i förhoppning om att de större lantanatomerna endast skulle byta ut europiumatomerna i en av de två grupperna. Ett sådant plats-selektivt byte av metallatomer skulle medföra att en av de två topparna skulle försvinna, då lantan inte absorberar synligt ljus. Den topp som var kvar skulle då kunna härledas till de två europiumatomer som inte bytts ut mot lantan, medan den som försvunnit skulle höra till de europiumatomer som bytts ut mot lantan.

Röntgendiffraktion visar dock på att lantan har bytt ut europium till 50% på båda platserna (i stället för 0% på den ena och 100% på den andra platsen). Även i spektroskopimätningarna syns fortfarande en dubbel topp. För att uppnå önskad effekt skulle man behöva en större jonradieskillnad, som t.ex. den mellan europium och den betydligt mindre skandiumatomen.

$Eu_3K_3TiO_2(OMe/OH)(O^tBu)_{11}(HO^tBu)$

Med tertbutoxidjon ($^-O^tBu$ = $^-OC(CH_3)_3$) som ligand har ännu inga europium-titan-oxo-alkoxider framställts. I ett försök bildades dock en europium-kalium-titan-oxo-alkoxid. Kalium används i syntesernas första steg och ersätts normalt under syntesens gång med europium, men i detta fall har uppenbarligen inte allt kalium kunnat bytas ut mot europium. Med hjälp av röntgendiffraktion bestämdes molekylstrukturen. Detta visade på ytterligare en oväntad händelse: värmebehandling har orsakat sönderfall av en del av tertbutoxidjonerna till metoxidjoner (^-OMe = $^-OCH_3$) eller hydroxidjoner (^-OH), vilket gör att formeln blir $Eu_3K_3TiO_2(OMe/OH)(O^tBu)_{11}(HO^tBu)$.

I varje molekyl finns två centrala syreatomer: en som koordinerar sex metallatomer (tre europiumatomer och tre kaliumatomer) och en som koordinerar fyra metallatomer (samma tre kaliumatomer och en titanatom). Att två oxo-ligander delar på samma tre metallatomer är ovanligt i denna typ av molekyler.

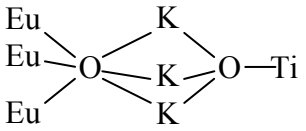

Fig. 5 Omgivningen runt oxoliganderna i $Eu_3K_3TiO_2(OR)_{12}(HOR)$

Likt $Eu_2Ti_4O_2(OEt)_{18}(HOEt)_2$ innehåller även $Eu_3K_3TiO_2(OMe/OH)(O^tBu)_{12}(HO^tBu)$ en alkoholmolekyl som för röntgenstrålningen ser ut precis som en alkoxidjon, då väteatomen är för obetydlig. Ibland kan man från molekylens geometri dra slutsatser kring var det sitter en eventuell alkoholmolekyl i stället för en alkoxidjon, men i fallet $Eu_3K_3TiO_2(OMe/OH)$-$(O^tBu)_{12}(HO^tBu)$ har en noggrann analys av strukturen inte lett till någon ledtråd angående vilken av tertbutoxidjonerna som i själva verket är en tertbutanol-molekyl.

Sammanfattningsvis har fyra europium-titan-oxo-alkoxidstrukturer beskrivits, varav en med en helt ny strukturtyp med intressanta egenskaper. Därmed har ytterligare några pusselbitar lagts i riktning mot ökad förståelse av oxo-alkoxidstrukturer, vilket i förlängningen kan leda till vidareutveckling av syntesmetoder som ger nya eller förbättrade materialegenskaper.